Systemic inflammation causes microglial dysfunction with a mixed AD-like pathology

Praveen Bathini
University of Fribourg Faculty of Science and Medicine: Universite de Fribourg Faculte de sciences et de medecine

Isabel Dupanloup
Swiss Institute of Bioinformatics

Elena Zenaro
Universita degli Studi di Verona Dipartimento di Medicina

Eleonora Terrabuio
Universita degli Studi di Verona Dipartimento di Medicina

Amrei Fischer
University of Fribourg Faculty of Science and Medicine: Universite de Fribourg Faculte de sciences et de medecine

Edona Ballabani
University of Fribourg Faculty of Science and Medicine: Universite de Fribourg Faculte de sciences et de medecine

Marie-Agnes Doucey
University of Lausanne Faculty of Biology and Medicine: Universite de Lausanne Faculte de biologie et medecine

Lavinia Alberi Auber (lavinia.alberi@unifr.ch)
Swiss Integrative Center for Human Health https://orcid.org/0000-0002-0446-5337

Research

Keywords: Inflammation, PolyI:C, brain aging, microglia, sporadic Alzheimer's disease, Vascular dementia,

Posted Date: January 18th, 2021

DOI: https://doi.org/10.21203/rs.3.rs-145868/v1

Abstract

Background Alzheimer's disease (AD) is the primary cause of cognitive deficit in elderly humans. Late-onset AD (LOAD) is sporadic, multifactorial, and non-Mendelian accounting at present for 95% of the cases in contrast to the genetic form of the disease. Risk factors for sporadic AD include Gene: Environment interactions. There is increasing evidence that lifestyle and stress such as viral or bacterial infection causing chronic inflammation are underlying culprits of neurodegenerative dementia. Dementias that share or mimic pathological processes of AD include cerebrovascular diseases, Lewy body disease, TDP-43 proteinopathy. To date, very few mouse models reproduce the pathophysiological progression of mixed-vascular-AD, while the majority of studies have employed transgenic animals reproducing the familial form.

Methods We have re-engineered the Polyinosinic:polycytidylic acid (PolyI:C) sterile infection model in wildtype C57BL6 mice to achieve chronic low-grade systemic inflammation. We have conducted a cross-sectional analysis of aging PolyI:C and Saline control mice (3 months, 6 months, 9 months and 16 months), taking the hippocampus as a reference brain region, based on its vulnerability, and compared the brain aging phenotype to AD progression in humans with mild AD, severe AD and Controls (CTL), in parallel to Vascular dementia (VaD) patients' specimens.

Results We found that PolyI:C mice display both peripheral and central inflammation with a peak at 6 months, associated with memory deficits. The hippocampus is characterized by a pronounced and progressive tauopathy. In PolyI:C brains, microglia undergo aging-dependent morphological shifts progressively adopting a phagocytic phenotype. Transcriptomic analysis reveals a profound change in gene expression over the course of aging, with a peak in differential expression at 9 months. We confirm that the proinflammatory marker *Lcn2* is one of the genes with the strongest upregulation in PolyI:C mice upon aging. Validation in brains from patients with increasing severity of AD and VaD shows a reproducibility of some gene targets in vascular dementia specimens rather than AD ones.

Conclusions The PolyI:C model of sterile infection demonstrates that peripheral chronic inflammation is sufficient to cause neuropathological processes resembling a mixed-VaD-AD phenotype, with progressive tau hyperphosphorylation, changes in microglia morphology, astrogliosis and gene reprogramming reflecting increased neuroinflammation, vascular remodeling and the loss of neuronal functionality seen to some extent in humans.

Background

Alzheimer's disease (AD) is the most common form of dementia, with vascular dementia (VaD) accounting for the second most frequent mixed pathology with AD (Toledo et al. 2013; Lin et al. 2019; Santos et al. 2017). While the familial and less common form of AD (FAD) has been linked to the mutations in the amyloid precursor protein (APP) and presenilin-1 &2 genes (PS1 and PS2), the etiology of late-onset or sporadic AD affecting people over 65 years of age shows the involvement of both genetic

and environmental factors. Underlying the pathogenesis of the disease, a large proportion of genetic factors, such as ABCA7, APOE, BIN1, CD2AP, CD33, CLU, CR1, HLA-DRB1, and SORL1 (Barber 2012) are immunological factors. Furthermore, APOE and SORL1 have been previously associated with Cerebral Amyloid Angiopathy (CAA) (Du et al. 2019) supporting vascular inflammation as a comorbidity factor accelerating the progression of AD (Thal et al. 2002). In addition to the host immunotype, exposure to microbial pathogens (viruses, bacteria, fungi, etc) can potentiate neuroinflammation and accelerate neuropathological events like AD (Sochocka, Zwolińska, and Leszek 2017). Spirochetes, Chlamydia Pneumoniae, Porphyromonas Gingivalis and Herpes Simplex Viruses (HSV-1, HSV-2, and HHV-6) are enriched in the brains of AD patients and their titer correlates with the progression of the disease (Fulop et al. 2018). The casual relationship between viral infection and the development of AD has been recently supported by retrospective observational studies looking at the protective role of antiviral drugs for dementia (Tzeng et al. 2018). Interestingly at least two reports show that viral infections are more recurrent in APOEε4 carriers, bearing a higher risk of dementia conversion with aging (Linard et al. 2020; Itzhaki and Wozniak 2006).

Further, epidemiological studies indicate maternal infections as one of the priming event for chronic neuroinflammatory responses (Li et al. 2018), representing a major risk factor for neurodevelopmental disorders in the offspring (Conway and Brown 2019; Bilbo et al. 2018) and neurodegenerative diseases such as Parkinson's disease (Carvey et al. 2003) or AD later in life (Hoeijmakers et al. 2016; Knuesel et al. 2014). Studies in animals confirm that prenatal viral infection induces neuroinflammation and cognitive deficits (Ito et al. 2010) and that recurrent infections may cause an Alzheimer's like phenotype (Little et al. 2004; Dominy et al. 2019; De Chiara et al. 2019). Previous animal studies using PolyI:C (Polyinosinic:polycytidylic acid), a synthetic double stranded RNA induces viral-like inflammation through toll-like receptor 3 (TLR3) signaling (Ting 2001), reported that late prenatal viral-like immune activation was enough to induce chronic inflammation and predisposes the offspring to AD-like neuropathology (Kristic et al. 2012). This evidence was later rejected in a work showing that prenatal immune insults with PolyI:C can induce only transient inflammatory response despite producing cognitive impairments in the injected mice (Giovanoli et al., 2015). Taking into consideration the evidence supporting a role for chronic inflammation in AD but also the discrepancies on the effect of viral immune challenge in the development of AD, we readapted the PolyI:C mouse model to achieve a chronic systemic inflammation in naive mice by two injections, one in late pregnancy and the second in the young adult offspring. In our experimental paradigm, the early second immune challenge bolus was hypothesized to achieve sustained chronic inflammation deviating from the original model (Krstic et al. 2012) that could not be replicated by other studies (Giovanoli et al. 2015). The new optimized PolyI:C mouse model reveals long term systemic & central immune response resulting in significant proteinopathy associated with spatial memory deficit, microglia remodeling, transcriptomic changes leading to increased lipid metabolism and vascular factors activation, resembling a mixed vascular-AD pathophysiology. Our findings further consolidate the link between an imbalance of the immune system and the pathogenesis of AD (Morgan et al. 2019; Engelhart et al. 2004; Leung et al. 2013), with peripheral inflammation prompting central immune responses (Perry, Cunningham, and Holmes 2007) and causing neurodegeneration in the long-term (Saeed et al. 2014).

Materials And Methods

Animals

Wildtype C57BL/6J mice were used for the study. Animal experimentation was approved by the animal experiment committee, University of Fribourg (Protocol no. 2016_32_FR registered 01/01/2017). The animals were fed ad libitum and housed in a room equipped with automatically controlled temperature (21-25°C), humidity (50%), and with a 12 hrs light/dark cycle.

Ethical Approval and Consent to participate

Frozen Human tissue samples from the entorhinal cortex including the hippocampal area were procured from the Medical Research Council Brain Bank for Dementia Research, Oxford, UK, and Stanford brain bank. We received frozen hippocampal brain tissue samples from 9 controls, 5 moderate, and 10 Severe sporadic AD patients (Suppl. Table 1). The use of human tissue has been approved by the Ethical Commission of the Brain Bank for Dementia UK (OBB443 registered 1/05/2017 and OB344 registered 1/02/2014), Stanford (Stanford IRB), and the Ethical Commission from the Canton of Fribourg and Vaud (N. 325/14). Vascular dementia hippocampal specimens and healthy age-matched controls were obtained from the Netherlands Brain Bank (NBB. 1251). All experiments conducted on human tissue comply with the WMA Declaration of Helsinki.

Treatment

To investigate the early postnatal treatment and microglial priming the systemic PolyI:C challenges were optimized from the already existing model with PolyI:C (Krstic et al. 2012). Female C57BL/6J mice 6-8 weeks old were housed together with the males for mating. Vaginal plugs were assessed and pregnant mice with gestation day (GD) 17 were injected intravenously (i.v.) with 5mg/kg PolyI:C (Polyinosinic-polycytidylic acid; P9582, Sigma, USA). Aliquots of 5mg/ml were prepared by resuspending in the sterile 0.9% saline and were stored at -20°C until further use. For control experiments sterile 0.9% saline was used. To mimic chronic or recurrent inflammatory responses to systemic viral infections like in humans, prenatally challenged offspring were given a second immune challenge with an intraperitoneal (i.p.) PolyI:C injection at 20mg/kg dose or sterile saline for the control experimental mice (Fig. 1A). For all the subsequent experiments adult male offspring were used in the study.

Behavioural experiments

In this work, we characterized age-related changes in the mice behavior throughout aging i.e., from young adulthood to aged mice. Anxiety was tested at 3, 6, 9, and 16 months of age in PP mice (Prenatal and Postnatal PolyI:C injected) and NN mice (Prenatal and Postnatal saline injected) using the Open field test registering the time spent in the center, while elevated O-maze was used at 3 to 6 months only recording both the time spent in the open unprotected arm and time spent in the light. Working memory was tested using the Y-maze alternation task and expressed as % of alternation and number of arm entries during a 5 minutes exploration-window according to previously published protocols (Crawley and Bailey 2008;

Miedel et al. 2017). Behavioral tests were videotaped and videos were analyzed using Image J-built in macros for automated video-tracking (Supplementary Material and Methods) (Brai and Alberi 2015).

Tissue Processing

Animals were first deeply anesthetized with pentobarbital sodium (100mg/kg, i.p) and verified with toe pinch pain reflex. After the abdominal opening, mice were transcardially perfused with 0.9% sterile saline, brains were harvested and cut into two hemispheres. One hemisphere was dissected to collect the hippocampus and further dissected in an ice-cold saline solution to obtain the Corpus Ammonis (CA) fields, removing the dentate gyrus (Brai et al. 2015). The tissue samples were collected into eppendorfs and were flash-frozen in liquid nitrogen and stored at -80°C until further use. The other hemisphere was post-fixed in 4% PFA for 1 day, followed by immersion in 30% sucrose at 4°C and then embedded in an OCT block for cryosectioning at 35µm thickness (Leica, Germany) and used for histological studies.

Plasma collection

The whole blood collected via cardiac puncture was transferred into the EDTA-coated eppendorfs. Cells were separated from the plasma by centrifugation for 15 min at 2000 x g at 4°C before extracting the plasma. The plasma samples were then stored at -80°C until further use.

Isolation of leukocytes from mouse tissues and Flow cytometry

Blood: Mice were anesthetized via isoflurane inhalation. Blood samples were collected through a retro-orbital non-surgical procedure by sodium heparinized capillaries. Dextran 1% and Heparin 10 U/ml were added to the blood in a 1:1 ratio. After erythrocytes sedimentation (1 hour), the overlying supernatant plasma-dextran suspension of leukocytes was washed in 1X PBS. Red blood cell lysis was performed adding 3 ml of NaCl 0.2% for 40 seconds and then 7 ml of NaCl 1.2%. Next, cells were washed and stained.

Brain: Mice were anesthetized and quickly perfused through the left cardiac ventricle by injection of cold PBS 1X Ca_2Mg_2 1 mM. After meninges removal, brains were collected. Mechanical digestion through gentleMACS^{TM} Octo Dissociator (Miltenyi Biotec) and subsequent enzymatic digestion with 2 mg/ml of collagenase (C0130; Sigma-Aldrich, USA) and 40 U/ml of DNase (EN0521; Invitrogen, Life Technologies, USA) at 37°C for 45 minutes in water bath were performed. Cells were isolated by passing the digested tissue through a 70-mm cell strainer, resuspended in 30% Percoll (GE Healthcare, USA), and loaded onto 70% Percoll (GE Healthcare, USA). After centrifugation at 2500 rpm for 20 minutes at 4°C, cells were removed from interphase, washed, and stained.

Cells were treated with an antibody against Fc receptor [anti-mouse CD16/32, Clone: 2.4G2; Becton Dickinson (BD), USA] and labelled with BD Horizon Brilliant^{TM} Stain Buffer (BD, USA) to improve staining quality and with 2.5 ml per sample of each of the following anti-mouse mAbs: Ly6G BB515 (Clone: 1A8; BD, USA), CD45 BV786 (Clone, 104 RUO; BD, USA), CD11b BV421 (Clone: R1-2; BD, USA), F4/80 (Clone:

T45-2342 RUO; BD, USA), CD11c BV 605 (Clone: HL3; BD, USA), Siglec F PE (Clone: S17007L; BD, USA), B220 APC (Clone: RA3-6B2 RUO; BD, USA). Cells were stained for 15 minutes at 4°C in the dark according to the manufacturer's instructions. After washing, cells were incubated with 7AAD (BioLegend, USA) fluorescent intercalator for 5 minutes at 4°C in the dark. Samples were acquired through LSRFortessa X-20 (BD, USA). Data was analyzed through FlowJo™ Software. In particular, after doublets removal, $7AAD^-$ alive cells were selected. A specific gating strategy was used to identify subpopulations of leukocytes in blood and brain samples. The following $CD45^+$ cell populations were detected and analyzed: $Ly6G^+$ $CD11b^+$ $B220^-$ Neutrophils, Siglec F^+ $CD11b^-$ $CD11c^-$ Eosinophils, $F4/80^+$ $CD11b^+$ $SiglecF^-$ Monocytes. Using the DownSample Plugin developed by FlowJo™ (https://docs.flowjo.com/seqgeq/dimensionality-reduction/downsample/), the number of $CD45^+$ events in data matrix was reduced to a maximum of 30.000.

Bead-based Immunoassay

To study the PolyI:C effect on plasma inflammatory profile, we measured chemokines IL-6, IL-10, MCP-1, and TNF-α using the premixed inflammation panel (PN: C282251A, Aimplex Biosciences, USA) according to the manufacturer's instructions. Briefly, 45 µl of the capture bead working solution, 30 µl of assay buffer, and 15 µl of the sample were incubated on the shaker (700 rpm) for 60 minutes at room temperature. After 3 washes with 100 µl washing buffer, 25 µl of biotinylated antibody working solution was added and incubated on the shaker for 30 min at room temperature with protection from light. After 3 washes, 25 µl of streptavidin-phycoerythrin working solution was added, shaken for 20 minutes in the dark. Finally, the beads were resuspended on 150 µl of 1x reading buffer and read on Flow Cytometry Analyzer (LSR-IIa; BD, USA) acquiring about 50 events per chemokine. The FCS files were analyzed on Flowing software (http://flowingsoftware.btk.fi/) and the cytokines' and chemokines' levels were determined based on 5-parameter logistic curve fitting.

Immunoassay of Amyloid-β_{1-42}

Frozen cortical tissue samples were homogenized with lysis buffer containing 20 mM Tris-HCl (pH 7.5), 150 mM NaCl, 1 mM disodium EDTA, 1 mM EGTA, 1% Triton, 2.5 mM sodium pyrophosphate, 1 mM β-glycerophosphate (G9422; Sigma, Germany), phosphatases inhibitor such as Sodium Orthovanadate (1mM, 450243; Sigma, Germany) and proteases inhibitor cocktail 1:100 (3749.1, Roth, Germany) and the lysates were stored at -80°C until further analysis. The sample and reagents preparation has been carried out according to the Milliplex Map kit Human Amyloid and Tau Magnetic Bead panel (Cat.# HNABTMAG-68K) manufacturer's protocol. Briefly, cortical lysates were diluted 1:2 with assay buffer. Standards, controls and samples were added to the appropriate wells of the 96 well filter plate. Biotinylated detection antibodies and magnetic mixed antibody-immobilized beads were added, sealed with aluminum foil, and incubated overnight in the dark at room temperature on a shaker (700rpm). The next day following washes, Streptavidin-phycoerythrin was added and incubated in the dark for 30 minutes at room temperature on a shaker (700rpm). Finally, the beads were suspended in 100 µl Sheath fluid and transferred to the 96 well flat bottom plate to be read on the FlexMap 3D system equipped with xPONENT

software (Merck, Germany). The median fluorescence intensity (MFI) was analyzed using a 5-parameter logistic curve-fitting method and analyte concentrations were calculated.

Nucleic acid and protein extraction

Fresh frozen hippocampal tissue specimens from mice and humans are stored at -80°C until utilized for RNA extraction using peqGOLD TriFast^{TM} (peqGOLD, Germany) according to the manufacturer's instructions to obtain RNA and proteins. The RNA pellet was extracted from the aqueous phase, air-dried, resuspended in 25µl of nuclease-free water (Promega). The concentration of the RNA samples was measured using the Qubit 3.0 Fluorometer (High sensitivity, Invitrogen) and stored at -80°C until further use. Proteins were extracted from the organic phase, cleaned with Ethanol, and the dried pellet resuspended with a 150 µl buffer containing 8M Urea in 4% (w/v) CHAPS and protease inhibitor (1:100 Carl Roth, Germany). The protein concentrations were determined using the Bradford assay method (Roth, Germany) and later the samples were stored until use at -80°C.

RNA library preparation and sequencing

Synthesis and amplification of cDNA were performed as per the Illumina TruSeq Stranded mRNA protocol. RNA extracted from the hippocampal specimens from all the age groups (3m, 6m, 9m, 16m) was used for this transcriptomics study. RNA integrity was determined with the Fragment Analyzer 5200 (Agilent). Samples with RNA integrity number (RIN) > 8 were used for the experiment. An input material of 1 µg of total RNA from each sample was used for library preparation with Illumina TruSeq Stranded mRNA kit (Cat: 20020595). Illumina TrueSeq Combinatorial dual (CD) indexes were used during the ligation, DNA fragments enriched using the PCR to amplify the amount of DNA in the library. The quality of the libraries is determined using the Standard High sensitivity NGS Fragment analysis kit (DNF-474, 1-6000 base pair) on the Agilent Fragment analyzer (Agilent, USA), yielding approximately 260 bp size fragments. The cDNA libraries were pooled in equivalent amounts. The libraries were denatured and diluted using standard library quantification and quality control procedures recommended as per the NextSeqprotocol. For a sequencing control, PhiX library was prepared and combined with the pooled prepared libraries. A final concentration of 1.5 pM library was sequenced on Illumina NextSeq 500 system (High output 150 cycles) to generate 20 million of 2 x75 bp pair-end reads per library.

Bioinformatics Analysis

In brief, hippocampal paired-end libraries from all the age groups (3m, 6m, 9m, 16m) in the saline treated and PolyI:C treated mice (n=3 each) were sequenced for the study. To generate the differentially expressed transcripts from the RNA sequencing data the following bioinformatics analysis pipeline was performed. 1) Remove adapter sequences and remove low quality (flanking N) bases from each read using cutadapt version 2.3; 2) Alignment of the reads to the reference genome using RNA-seq aligner STAR version 2.6; 3) Get basic alignment stats with RSeQC version 2.6.4; 4) Get read distribution with RSeQC version 2.6.4; 5) Get gene body coverage with RSeQC version 2.6.4; 6) Get read counts for genes with htseq-count release_0.11.1; 7) perform differential expression analysis with DESEQ2.

Further functional enrichments were performed using the ClueGO (Bindea et al. 2009) which integrates Gene ontology (GO), KEGG (Kyoto Encyclopedia of Genes and Genomes), Wikipathway, and Reactome pathway analysis creating a functional pathway network.

Reverse transcription-polymerase chain reaction (RT-PCR)

1µg of total RNA from the human and mouse brain specimen was reverse-transcribed using the M-MLV reverse transcriptase (Promega) for efficient synthesis of the first-strand cDNA. Gene expression analysis was done by RT-PCR (GoTaq qPCR Master Mix, Promega, USA) using gene specific primers (Suppl. Table 3) on Mic qPCR Cycler (BioMolecular Systems, USA). Expression levels of genes of interest were determined using the ΔΔCT method; the levels of the mRNAs of interest were normalized against the levels of the housekeeping gene, β-actin.

Antibodies & reagents

The following antibodies were used for western blot immunolabeling and immunohistochemistry experiments in this study:

Rabbit anti pTau 231 (1:500, ab151559, Abcam, UK), Rabbit anti pTau 205 (1:500, ab181206, Abcam, UK), goat anti-tau (1.25 µg/mL; AF3494, R&D systems, USA), mouse anti-β actin, 1:2000 (sc-81178; Santa Cruz Biotechnology, USA), Rabbit anti GFAP (1:500, ab68428, Abcam, UK), Goat anti GFAP (1:500, SAB2500462, Sigma), Goat anti Iba1 (1:500, ab5076, Abcam, UK), Mouse anti-amyloid-β6E10 clone (antibody recognizing the amino acid region 1-16 (Aβ1-16); 1:500, cat:803014; Biolegend, USA), rabbit anti-synaptophysin (1:500; ab14692, Abcam, UK), Rabbit anti-amyloid-β 42 (Aβ1-42; 1:500; D54D2 XP, Cell Signaling, USA), Rabbit anti-Lipocalin-2/LCN2 (1:500, 50060-RP02; Sino Biological, China), mouse anti-NF200 (1:500, cat:1178709; Boehringer Mannheim Biochemica, Germany), Nile Red (2 µg/mL, N3013, Sigma, USA), Thioflavin-S (100 mM; CAS 1326-12-1, Santa Cruz Biotechnology, USA)

The secondary antibodies used in the study for immunolabeling were: directly conjugated to Cy2, Cy3, or Cy5 raised in donkey (all 1:1000; Jackson Immuno Europe, UK). DAPI (4',6-diamidino-2-phenylindole, Cat. no. 10236276001 Roche, Switzerland) was used to visualize nuclear morphology.

Western blot

Hippocampal lysates were denatured at 95°C using the 2-Mercaptoethanol based loading buffer. Proteins were separated using the SDS-polyacrylamide gel electrophoresis and western blot procedure. Custom made 8-10% gels were used to run the samples for 1.5 hours at 110 voltage. The proteins were then transferred to a precut 0.2 µm nitrocellulose membrane (Cat: 1620146; Biorad, USA) using a wet transfer method (Biorad). Later the membranes were incubated in a blocking solution containing 0.5% bovine serum albumin (Art. No. 8076.4, Roth, Germany), 1xTBS, and 0.1%Tween-20 for 30 minutes at room temperature on a rotating shaker. The membranes were then incubated with primary antibodies overnight at 4°C with gentle agitation. On the second day, the membranes were rinsed with TBS-Tween solution 3 x 5 minutes, followed by a 1-hour incubation with the fluorescently conjugated secondary antibodies, rinsed

again and air-dried covered by aluminum foil. The proteins were detected using the Omega Lum (Labgene, CH). The optical density of the protein bands was determined using Image J software and normalized to the Beta-actin control. For an accurate total protein quantification REVERT stain (LI-COR Biosciences-GmbH, Germany) was also employed.

Fluorescent immunohistochemistry

The mice sagittal tissue sections from the anti-freezing medium were taken and then mounted onto the superfrost glass slides, air-dried for 1 hour, and washed twice in Distilled water 5 minutes each. To access epitopes slides were incubated at 65°C (water bath) for 20 minutes in 10mM Sodium citrate (pH 6) containing 0.05% Tween (Preheat buffer). Thereafter, sections were washed 3 times 5 minutes each in 1x Trizma-based salt solution (TBS), at room temperature, and once in a TBST buffer (1x TBS containing 0.1% Triton solution). Sections were blocked in the blocking solution (TBST buffer containing 10% fetal bovine serum) for 1 hour at room temperature in a humid chamber. Further, the sections were incubated with the primary antibody in the TBST buffer containing 1% fetal bovine serum at 4°C in the refrigerator overnight. The next day, sections were washed 3 times for 5 minutes each in the TBS buffer before being incubated with the fluorescently labeled secondary antibodies for 3 hours at room temperature. Following the labeling, the sections were washed 3 times in 1x TBS buffer, 5 minutes each. In one staining (pTau and Thioflavin S), sections were incubated with Thioflavin S, followed by 2 x 5 minutes washes with distilled water. After the last wash, sections are incubated with for 10 minutes at room temperature. Thereafter, the sections were washed 2 times, 5 minutes each with TBS, and mounted with custom-made aqueous mounting media containing 1,4-Diazabicyclo[2.2.2]octane (803456 EMD Millipore, USA). For the lipid droplet Nile red staining, sagittal brain sections were mounted onto the glass slide and air-dried, followed by a rinse with deionized water for 1-2 minutes. Nile red/glycerol staining solution (2µg/ml) was added onto the tissue, incubated for 5 minutes, and coverslipped before being examined using a confocal fluorescence microscope (Zeiss LSM 800, Germany).

Image quantification

To quantify the glial response to an increase in systemic and central inflammatory profile, the morphology of these brain innate immune cells has been analyzed. Iba-1 positive microglia images (10 ROI/section) were taken at 40x oil immersion objective using a Confocal microscope (Zeiss LSM 800, Germany) with 1 µm Z intervals resulting in stacks of 20-30 slices at 512 x 512 pixel resolution. The soma area, perimeter, circularity, skeleton analysis was performed as instructed (Young and Morrison 2018; Davis et al. 2017) and using custom-made macros (Suppl. Materials and Methods). For the Fractal analysis on aged mice microglia 60x Oil immersion objective was used to generate in-depth microglia morphological data. Mean fluorescence intensity (pTauT231) of the CA1 field was measured in the same age group using the ImageJ ROI manager. Amyloid-β and Lcn2 staining were analyzed for % area coverage using the custom-made ImageJ macros (Suppl. Materials and Methods). Nile red positive lipid droplets were analyzed using the Analyze particle function in ImageJ. For the histological data, ImageJ

macros were created and used for the analysis for an unbiased morphological quantification (Suppl. Materials and Methods).

Statistical analysis

Homogeneity of variance for each variable within a group age was verified by Levene's Test and comparative analysis performed either using the parametric test for normally distributed data (Student's t-test) or non-parametric test for non-normally distributed data (Mann Whitney test). Statistical significance was assessed using unpaired, 2-tailed Student's t-test and ANOVAs as specified in the figure legends. Results (mean ± SEM) were obtained using Excel Real Statistics plugin. *P* values less than 0.05 were considered significant. RNA sequencing data were analyzed using the RDESEQ2 package and statistically significant transcripts were chosen if p<0.05 and p adjusted for multiple testing <0.1. For the flow cytometry data, statistical analysis was performed through unpaired Welch's t-test using GraphPad Prism Version 8.1.2. Optical densities of immunoblots were compared between groups using ANOVA with Post-hoc Bonferroni correction. Morphology measurements of microglia were analyzed using the Kolmogorov–Smirnov test and in aggregate using Student's t-test. Correlation analysis was conducted using R and significance tested using Student's t-test.

Results

Chronic inflammation after double PolyI:C challenge

Double-challenged PolyI:C animals were injected in prenatal life at gestational day 17 and in the offspring at 2.5 months (PP). Animals were analyzed cross-sectionally at 3, 6, 9, and 16 months, taking saline-injected controls as reference (NN) (Fig. 1A). From 3 to 6 months of age levels of four circulating inflammatory cytokines (MCP-1, IL-6, TNF-α, and IL-10) are progressively higher in PP as compared to NN (Table 1). A two-way ANOVA highlights that the observed differences in the TNF α levels between treatment are due to the effect of age ($F_{3,37}$=95, p<0.001) based on the interactions between age and treatment ($F_{3,37}$=3, p<0.05), with higher levels in the 6 months PP mice than the other ages ($F_{1,14}$=9.4, p<0.005). We also observed a significant effect on IL-6 expression after PolyI:C treatment with aging ($F_{3,37}$=17, p<0.001) based on the interaction between treatment and age ($F_{3,37}$=17.59, p<0.00005) with a peak of plasma IL-6 levels in 9 months PP mice ($F_{1,8}$=71, p<0.00005). Later at 16 months, NN and PP mice show no difference in humoral immune factors (Table 1). Considering the upregulation of a large population of circulating chemokines in the blood of PP mice from 3 months of age, we examined the neutrophils, monocytes, and total polymorphonuclear cells (PMNs) from the freshly isolated whole blood and brain samples to study any infiltration of these leukocytes into the brain. Samples were analyzed using the flow cytometry for the expression of neutrophils and monocytes using antibodies stained for Ly6G, Siglec, F4/80, CD11b. Although no changes are observed at 3 months of age between groups, at 6 months PP mice exhibit elevated levels of neutrophils and PMNs in the systemic circulation but no significant differences are seen in the brain of PP mice as compared to NN animals (Suppl. Fig. 1A and

B). On the other hand, the monocyte population differs neither in the blood nor in the brain (Suppl. Fig. 1C).

While there is no trace of infiltrating immune cells in the brain at 3 or 6 months, analysis by RT-PCR of *IL-6* transcripts shows a significant different trend between PP and NN mice over time with aging ($F_{3,30}$=4.4, p<0.05) based on the interaction of treatment with age ($F_{3,30}$=10.9, p<0.005) After a peak at 6 months ($F_{1,8}$=1.5; p=0.05), *IL-6* decreases significantly in the brain of PP mice compared to saline controls ($F_{1,8}$=5.25, p<0.005). Further, *IL-1*β expression in PP brains changes overtime with aging ($F_{3,30}$=4.24, p<0.05), starting from lower levels in PP brains at 3 months ($F_{1,8}$=6.44, p<0.01) followed by a peak at 9 months ($F_{1,8}$=3.4, p<0.05). The effect of treatment on the expression of Interferon gamma (IFNγ), a cytokine critical against viral infections, showed a significant effect between the groups ($F_{1,30}$=4.7, p<0.05) and a slight difference over time ($F_{3,30}$=2.49, p<0.07) with a rise in expression of IFNγ in PP brains at 6 months as compared to NN ($F_{1,10}$=6.78, p<0.05).

We further analyzed how the inflammatory transcripts correlate with cell-type-specific transcripts for neurons (*GRIN1,* Glutamate Ionotropic Receptor NMDA Type Subunit 1), microglia (*Iba1;* Ionized calcium-binding adaptor molecule 1) and astroglia (*GFAP;* Glial Acidic Fibrillary Protein) in PP and NN animals. We observe that *GRIN1* expression is stable except for a trending increase at 9 months (Fig. 1C), whereas *Iba1* shows dynamic changes with a progressive increase from 6 to 9 months and drop at 16 months ($F_{1,8}$=5.9, p<0.05) (Fig. 1D) similarly to the proinflammatory cytokines (*IL-6*, r16mo=0.77 and *IL-1*β, r16mo=0.68). At 6 months ($F_{1,8}$=1.7, p=0.19) and 9 months ($F_{1,8}$=7.5, p<0.05), *GFAP* expression increases but decays to normal levels at 16 months (Fig. 1E). The temporal evolution of *GFAP* overlaps with that of IL-1β, (rt =0.62, p<0.05; Fig. 1F). Our results show that the combination of prenatal and an early postnatal PolyI:C immune activation causes a prolonged and sustained systemic inflammatory response with the recruitment of circulating leukocytes of the innate immunity, and increased neuroinflammation and gliosis at mid-age.

Progressive tauopathy in PP mice

Inflammatory mechanisms are central to AD pathology involving both the interaction between inflammatory stimuli, proinflammatory cytokines/mediators, and AD pathological hallmarks such as aggregates of Aβ and hyperphosphorylated tau protein (p-tau) (Kinney et al. 2018), underlying neural network dysfunction and brain atrophy. We determined the impact of systemic immune challenge on the pre-tangle pathology by analyzing tau hyperphosphorylation at positions 231 and 205 using western blot (Fig. 2A) and immunohistochemistry (Fig. 2F and Suppl. Fig. 2A) on hippocampal tissue from 3 to 16 months of age. The content of hippocampal p-tau (pTau T231) relative to total tau (ptau/tau) is significantly different between PP and NN ($F_{1,30}$=11.5, p<0.005) with aging ($F_{3,30}$=6.7, p<0.005) based on the significant interaction between treatment and age ($F_{3,30}$=5.6, p<0.005). Specifically, ptau/tau increases dramatically in PP mice at 6 months, ($F_{1,7}$=21.7, p<0.00005), remains elevated at 9 months ($F_{1,8}$=10.5, p<0.005) and then is indistinguishable from NN mice at 16 months (Fig. 2B and 2C). The

progressive tauopathy is confirmed by immunolabeling of pTau fibers (pTau T205) in the hippocampal CA1 region and CA1 stratum lacunosum (Suppl. Fig. 2A), with a significant increase in pTau pixels in the CA1 region at 16 months (Suppl. Fig. 2B). Tau hyperphosphorylation and the formation of β-sheet fibrils, labeled by Thioflavin-S, can be observed in the CA3 field at 9 months in PP mice, in contrast to NN (Fig. 2F). To assess whether the progressive tauopathy in PP is associated with synaptic abnormalities and neuroinflammatory responses, we quantified the levels of synaptophysin and GFAP overtime (Fig. 2D). At 16 months in PP mice, we observe a non-significant drop in synaptophysin expression accompanied by significant increase in GFAP ($F_{1,30}$=10.04, p<0.005) (Fig. 2E). The increase in GFAP immunoreactivity is confirmed by immunohistochemistry of the CA3 region showing the presence of amyloid-β1-42 and p-tau small aggregates (Fig. 2G; insert). Further analysis of amyloid-β fibrils in the 16 months old mice indicates that Aβ1-42 is also present in NN old mice with internalization in GFAP positive glial cells, which is more pronounced in PP mice (Fig. 3A, white stars). Besides, in 16 months old PP mice, Aβ1-42 positive aggregates are visible in vessels ensheathed by astroglial endfeet reflecting CAA (Fig. 3A, white arrows). Increased colocalization between insoluble Aβ1-42 and p-tau in 16 months old PP as compared to NN both in the hippocampus (Fig. 3A) and the entorhinal cortex (Fig. 3B). In the latter region, Aβ1-42/p-tau positive aggregates display a stellate morphology resembling core-plaques (Fig. 3C, insert). The number of plaques rises 4 folds in PP as compared to NN (Fig. 3D), with a 70% larger amyloid-β burden in the area examined (Fig. 3E). Quantification of soluble Aβ1-42 from the entorhinal cortex shows a peak in Aβ1-42 release at 6 months in PP mice which later subdues (Fig. 3F), possibly as a result of insoluble aggregate formation in the brain.

PolyI:C-induced memory impairment

Based on the proteinopathy in the hippocampal and entorhinal cortex region following double PolyI:C injection, we assessed whether spatial working memory is affected. Previous work has shown that spontaneous alternation, a form of working memory, is entirely dependent on hippocampal synaptic function (Pioli et al. 2014; McHugh et al. 2008). Same set of PP and NN animals were subjected to the Y-maze spontaneous alternation task at 3, 6, 9, and 16 months. The number of arm entries and sequence were recorded, and the percent alternation was calculated (Fig. 3G). Although the activity of PP treated animals increases in terms of alterations at 3 months, the percentage of alternation did not change at this age as compared to NN ($t_{(17}$= 0.76, P = 0.46; n = 10 for Control and n=9 for PolyI:C). On the other hand, deficits in the spontaneous alternation are observed in the PP group both *at* 6 months ($t_{(17)}$ = 3.21, p = 0.005, n = 10 for NN and n=9 for PP), 9 months ($t_{(15)}$ = 2.57, p = 0.013, n = 9 for NN and n=8 for PP) and 16 months ($t_{(13)}$ = 2.57, p = 0.02, n = 8 for NN and n=7 for PP). The number of arm entries in the Y maze task is not significantly different across all the age groups (Suppl. Table 4) indicating normal locomotory behavior representing a non-confounding factor for the percentage of an alternation. However, from 9 months of age both PP and NN display about half of the number of entries as compared to younger animals. Since early and late gestational PolyI:C treatment has been linked to stress and anxiety-like phenotypes relevant to schizophrenia (Hui et al. 2018; Silveira et al. 2017) we tested these mice for Light/dark, Elevated O-maze at 3 and 6 months and Open field tasks at all ages. We found no

difference in the anxiety-like behaviour (Suppl. Table 5) disambiguating the spatial memory impairments observed. Together the data suggest that prenatal and early postnatal viral-like immune activation through PolyI:C treatment causes proteinopathy of the limbic regions with sustained working memory impairment.

Activation and phenotypic change in microglia of PP animals

Earlier studies have shown that systemic infections and the subsequent peripheral immune activation have a strong effect on brain function, glial response representing a risk for dementia (Cunningham and Hennessy 2015; Cunningham 2013). Microglia cells are the primary phagocytic innate immune cells of the brain that get stimulated upon immune activation. They normally exist in a resting state displaying a ramified morphology, while in intermediate states display a bipolar or rod-like phenotype (Davis et al. 2017) and in an activated state an amoeboid, irregular shape (Ling and Wong 1993). Quantification of Iba-1 positive cells per mm^3 in the immunostained hippocampus (Fig 4A), indicates no difference between PP and NN at the different stages (Suppl. Table 6). Next, we assessed whether the PP brains show altered microglial cell morphologies reflecting an activated inflammatory status. We quantified morphological parameters like soma size, perimeter, circularity, skeleton analysis of Iba-1 positive microglia (Fig. 4), and finally we conducted the fractal analysis in NN & PP mice across staging. From 6 months of age, Iba-1 positive microglia show an increased ramified morphology as detected by immunofluorescence microscopy (Fig. 4A). Quantitative soma analysis shows a slight increase in the soma size, typical of activated microglia in PP mice at 3 months (22%, $t_{(359)}$=4.7, $p<0.005$), which lasts up to 9 months (58%, $t_{(109)}$=4.32, $p<0.005$) (Fig. 4B). The cell soma perimeter measurement shows dynamic changes at 3 months (11% increase, $t_{(354)}$=2.7, $p<0.01$), and a significant increase at 9 months (57%, $t_{(98)}$=4.5, $p<0.005$), while no changes are detected at 6 and 16 months (Fig. 4B). Circularity, which indicates the roundness index, shows a deviation from circularity in the intermediate ages at 6 months (10% decrease, $t_{(300}$=3.15, $p<0.005$), 9 months (21% decrease, $t_{(164)}$=3.9, $p<0.005$) and 16 months (10% increase, $t_{(81)}$=2, $p<0.05$), indicating signs of progressive microglial activation with aging (Fig. 4B). These dynamic changes were further analyzed using the distribution curve analysis which indicates an overall shift in the number of cells with an increase in microglial cells soma size and perimeter (Suppl. Fig. 3A-3B) with irregularly shaped cell body during the adult and mid-aged intermediate stages (6 and 9 months) while at later stages (16 months), microglia become more circular or rounded suggesting morphological fluctuations across staging and signs of microglial activation (Suppl. Fig. 3C). To further characterize the phenotypic changes in microglia, reflecting their activation state, we performed the skeletal analysis of Iba-1 positive microglia, at 3, 6,9, and 16 months in PP and NN mice. Skeletonized Iba-1 renderings reveal a significant increase in the number of endpoints/ cell, maximum branch length/cell, and branch length/cell (Fig. 4C) in PP mice with age groups 3 months to 9 months indicating hyper ramified microglia. At 3 months (endpoints/cell $t_{(94)}$=3.12, $p<0.005$; maximum branch length/cell $t_{(59)}$=2.45, $p<0.05$; branch length/cell $t_{(130)}$=0.4, $p=0.6$), 6 months (endpoints/cell $t_{(101)}$=1.84, $p<0.05$; maximum branch length/cell $t_{(116)}$=1.4, $p=0.1$; branch length/cell $t_{(98)}$=2.5, $p<0.05$) and 9 months (endpoints/cell $t_{(118)}$=3.52, $p<0.005$; maximum branch length/cell $t_{(115)}$=3.4, $p<0.005$; branch length/cell $t_{(118)}$=2.1,

p<0.05). However, at 16 months, microglia in PP brains show a significant drop in the number of endpoints/cells ($t_{(31)}$=2.7, p<0.05) and an overall decrease in the branch ($t_{(41)}$=0.2, p=0.8) and maximum branch length ($t_{(34)}$=1.48, p=0.1) (Fig. 4C). Therefore, prenatal and early postnatal systemic PolyI:C immune activation induces hyper ramified microglia in the offspring which later undergoes a transition from hyperactivated to more bushy or amoeboid with the reduction in microglial endpoints.

Having detected a microglia morphological transition in aged PP mice, confocal imaged microglia cells were further investigated using fractal analysis (FracLac plugin of ImageJ) which renders the shape of microglia cells and quantifies the parameters of cell area, cell perimeter, Span ratio, circularity, and fractal dimension, the latter reflecting pattern complexity. The fractal analysis revealed significant changes in hippocampal microglia parameters in the aged 16 months PP mice versus NN (Fig. 4D). Normal resting microglia are complex with a higher fractal dimension. In the PP mice total microglia cell surface area ($t_{(80)}$=43.65, p<0.005) and the perimeter ($t_{(75)}$=4.2, p<0.005) is reduced indicating a more compact shape (Fig. 4E-4F). Fractal dimension as a measure for complexity, circularity and as a measure for the roundness is also reduced ($t_{(62)}$=4.9, p<0.005) after immune activation (Fig. 4H-4I). On the other hand, the span ratio is increased ($t_{(79)}$=1.9, p=0.06) reflecting microglia elongation (ratio of cell length and width) (Fig. 4G). Span ratio and circularity are inversely proportional indicating an activated microglia state. Altogether, systemic inflammation through pre- and post-natal PolyI:C induces profound changes in microglia morphology indicating a shift from resting to an activated state in aged PP animals.

Dynamic remodeling of the hippocampal transcriptome

To understand the mechanisms underlying the spatial memory deficits and the pathophysiological processes associated with the proteinopathy, and neuroinflammation we performed a cross-sectional hippocampal bulk mRNA sequencing on 3, 6, 9, and 16 months PP and NN animals. The analysis reveals many differentially expressed genes (DEGs) in the hippocampus (log2 fold change cut-off:05, adjusted p<0.05) between treatments. The gene expression profiles as visualized in the volcano plot (Fig. 5A-5D), show that in aged animals differential expression is highest with a peak at 9 months, coinciding with the neuroinflammatory switch in microglia cells. A GO analysis contextualized to the synapse (SYNGO) (Koopmans et al. 2019) indicates a dynamic shift in DEGs from the presynaptic compartment at 3 months (Supp. Fig 4A) to the postsynaptic terminal at 9 and 16 months (Supp. Figure 4C and 4D), with a non-synaptic stage at 6 months (Supp. Fig 4B). At 3 months, out of 35 DEGs between PP and NN, 21 are downregulated, and 14 are upregulated (Fig. 5A). Gene ontology enrichment analysis (GEA) of the biological processes using a 5% false discovery rate indicates general repression in genes associated with synaptic transmission, calcium signaling, extracellular matrix organization, and secretion (Suppl. Table 7). Pathway analysis based on a composite KEGG, Reactome, WikiPathways dataset shows high interconnectivity between cellular cascades associated with extracellular matrix organization, chemical synaptic transmission, and calcium signaling (Suppl. Fig 5A). In the 6 months, out of 32 DEGs between PP and NN (Fig. 5B), 22 are downregulated, and 10 upregulated. A GEA indicates ongoing processes of morphogenesis and gliogenesis (Suppl. Table 7), with highly overlapping pathways (Suppl. Fig. 5B). At 9

months (Fig. 5C) out of 196 DEGs, 90 are downregulated, and 106 are upregulated. The GEA shows enrichment in several processes associated with vascular remodeling, neurogenesis, morphogenesis, cytokine response, and cell death (Suppl. Table 7). Pathway analysis indicates partially overlapping cellular cascades shared among focal adhesion, BMP signaling, MAPK signaling, and neuronal injury (Suppl. Fig. 5D) confirming the concurrent processes of morphogenesis and cell death at this stage. In the 16 months PP mice (Fig. 5D) from the 99 DEGs, 50 genes are downregulated and 49 genes are upregulated. GEA of the DEGs indicates enrichment in the response to metal ions, the reactive oxygen response, morphogenesis, the regulation of cellular proliferation, and the response to hormones (Suppl. Table 7). Pathways analysis shows less interconnected cascades implicated in potassium ion transmembrane transport, monocytes proliferation, lamellipodium organization, and glucose metabolism (Suppl. Fig. 5D).

To better understand the dynamic changes in the sterile infection model undergoing with age, we compared the significantly differentiated genes between PP and NN at the cross-sectional time points. As shown in the Venn diagram (Fig. 5E), the number of common genes that are uniquely and commonly affected in the hippocampus of 3, 6, 9, 16 months PP mice indicates a large number of overlapping gene sets between 9 and 16 months, while fewer genes are shared with earlier stages. In particular, 6 shared genes can be subdivided into 2 categories reflecting a progressive cell-communication dysfunction (I) and a proinflammatory drive (II) in aging PP mice. (I) Genes downstream of MAPK-signalling (*c-Jun*) (E. K. Kim and Choi 2010), NFKB-signaling (*Egr2;* Early growth response protein 2) (Williams et al. 1995), responsible for neuronal excitability (*Kcnj2;* Potassium Inwardly Rectifying Channel Subfamily J Member 2) (Binda et al. 2018), with reported association with synaptic dysfunction, are downregulated in PP mice starting from 6 months (Fig. 5F). (II) On the other hand, genes related to neuroinflammation such as the lipid-droplet dependent gene (*Plin4;* Perilipin 4) (Han et al. 2018), pro-inflammatory genes (*H2-Aa*; Immunohistocompatibility-complex) (Van Hove et al. 2019) and acute-phase proteins regulating to the inflammatory response (*Lcn2*; Lipocalin-2) (Dekens et al. 2020) are upregulated in aging PP mice, starting from 9 months (Fig. 5G). Overall, the gene remodeling across the aging continuum replicates processes typical of AD with neuronal network breakdown, altered immune response, chronic neuroinflammation and vascular dysfunction.

Substantial changes in brain metabolism and inflammation

We further validated the RNA-seq analysis via RT-PCR, on some of the significant DEG with a reported association to AD as well as genes belonging to the neuronal (I) (Fig 5H) and metabolic (II) (Fig 5I) gene groups. At 3 months, *Cacna1g* (Calcium Voltage-Gated Channel Subunit Alpha1 G), which was previously reported to decay with aging and regulate amyloid-β production (Rice et al. 2014), is unchanged (0.9) in contrast to the observed reduction via RNA-seq (Log2FC=-0.55), suggesting that aggregate changes rather than single-gene changes may contribute to the modeled conductivity dysfunction (Suppl. Tab. 7). As expected at this stage, *Plin4* and *Egr2* are unchanged, matching the RNAseq data (Table 2). At 6 months, we analyzed one of the genes with the strongest downregulation at the RNA-seq, with reported association with cognitive impairment in chronic cerebral hypoperfusion (Xie et al. 2018). The *Glpr2*

(Glucagon-Like Peptide 2 Receptor) decrease (80%), is confirmed (Table 2; p<0.05). Also, *Ide* (Insulin-degrading enzyme), which has been implicated in the clearance of insulin and amyloid-β (Qiu and Folstein 2006), show a comparable increase, between RNA-seq and RT-PCR analysis, but did not reach significance in the RT-PCR result (Table 2; p=0.16). Interestingly, *Kcnj2* shows a significant 2 fold increase at 6 months (Table 2; p<0.05), suggesting a modulatory K^+ currents effect. *Plin4* remain unchanged between PP and NN at 6 months in both analyses (Table 2). At 9 months, the reduction in *c-fos*, *c-Jun*, *Notch1*, *Kcnj2*, *Egr2*, and the increase in *Lcn2* can be confirmed at the RT-PCR, while *Plin4* show a non-significant increase using RT-PCR (Table 2; p=0.24). At 16 months, *Lcn2, Plin4* trends are reproduced according to the RT-PCR, while *Kcnj2* shows a comparable but not significant decrease (Table 2; p=0.36). The data indicates that around ¾ of the RNA-seq outputs could be replicated via RT-PCR validation, confirming the robustness of the bulk RNAseq discovery method and emphasizing that aggregate dataset can explain ongoing cellular and molecular processes in such models. Validated DEG profiles of *Kcnj2*, *Egr2,* and *Plin4* and *Lcn2* are matched with the expression of genes specific for neurons (*Grin1*), microglia (*Iba1*) and astroglia (*GFAP*) at 9 and 16 months to investigate associations of the selected genes in specific cell types (Fig. 5J). *Grin1*, *Iba1,* and *GFAP* are positively associated with their peaking trend at these time points (Fig. 1C-E) supporting the neuro-glia interplay. On the other hand, *Egr2* which decreases at 9 months and increases at 16 months is inversely correlated to *Grin1*, *Iba1,* and *GFAP* suggesting a potential ubiquitous regulation of this transcription factor on the cell-type-specific changes. Finally, *Plin4* and *Lcn2* are positively associated with their increasing trend from 9 to 16 months, confirming the RNAseq data and supporting the subsequent investigation of these neuroinflammatory markers in aged PP mice. Based on downregulation of *Glpr2* in adulthood, indicating vascular hyperperfusion (Xie et al. 2018) and the subsequent upregulation of the vascular and inflammatory markers, *Lcn-2*, at 9 months, we investigated vascular integrity by validating the gene expression of Kruppel-like factor 4, *Klf-4*, at 9 and 16 months and observed a transient downregulation at 9 months (Table 2). At the same time point, angiogenesis markers such as Cytochrome P450 Family 1 Subfamily B Member 1, *Cyp1b1,* and Angiopoietin-like 4, Angptl4, with reported function in vascular homeostasis and alteration in AD (Chakraborty et al. 2018; Ghosh et al. 2016) showed a peak at 9 months, supporting pathological vascular processes in aged adult PP mice.

Nevertheless, an increase in Lcn2 has been reported in both AD brains (Dekens et al. 2018; Naudé et al. 2012) and CSF from vascular dementia patients (Cerebrospinal Fluid) (Llorens et al. 2020a) raising the possibility that this molecule can capture a mixed vascular-AD pathology. In line with our PolyI:C model of sterile infection, the increase in Lcn-2 is likely attributed to the production and release by activated microglia, reactive astrocytes, neurons, and endothelial cells in response to inflammatory and infectious insults (Jha et al. 2015). Our immunofluorescence analysis using an antibody specific for Lcn2 shows an increase in Lcn2 protein expression in the hippocampal CA3 field of the PolyI:C mice at 9 months and 16 months aged mice (Fig. 6A). At 16 months, small Aβ1-42 aggregates are visible in the PP hippocampus in close association with Lcn2 positive cells (Fig, 6A, insert). Quantitative analysis of the Lcn2 signal shows a significant increase in the % of the Lcn2 stained area in PP mice in both age groups (9 months, $t_{(25)}$=4.2, p<0.005; 16 months, $t_{(62)}$=2, p<0.05) (Fig. 6B). To study lipid metabolism and intracellular lipid

droplets accumulation, as a sign of neuroinflammation with aging, we have utilized the dye Nile Red which accumulates in lipids and emits red fluorescence (Greenspan, Mayer, and Fowler 1985). We observed more Nile Red-positive lipid droplets (LDs) in the hippocampal CA3 field with aging, which is even more evident in PP mice as compared to saline controls (Fig. 6C). Triple labeling with Nile Red, Neurofilament L-200, and Iba1, shows that both NF200 positive neurons and Iba1 positive microglial cells have increased lipid droplets (Fig 6D). Quantitative analysis of the LDs, represented as fold change between the PP and NN at the different time points indicates that the density of the LDs is significantly greater in PP mice starting from 3 months, resulting in increased stained area, peaking at 6 months ($t_{(16)}$=2.6, p<0.05) (Fig. 6E). On the other hand, LDs' size shows a small but significant expansion (30%, $t_{(16)}$=3.14, p<0.05) in PP mice at 3 months but afterward remains unchanged between conditions (Fig. 6E). The histo-anatomical analysis confirms the presence of neuroinflammatory markers that contribute to an AD-like neuropathological progression.

Translation to Alzheimer's disease

To assess whether the newly designed PolyI:C model is reproducing genetic changes in human AD, we performed targeted fingerprinting focusing on a cross-sectional cohort of post-mortem entorhinal cortices containing the hippocampus from age-matched subjects with mild-moderate AD, severe AD and age-matched healthy controls (CTL) (Table 3 and Suppl. Table 1). We first examined cell-type-specific genes, *GFAP*, *Iba1,* and *MAP2*. Consistently, with our model we observe a progressive increase in *GFAP* expression from Moderate to Severe AD ($F_{2,21}$=9.29 p=0.012; Fig. 7A and Suppl. Table 8), while *Iba1* and *MAP2* remain unchanged (Fig. 7A and Suppl. Table 8). Next, we examined some of the relevant DEG with reported association with AD and divided them into functional categories. *Glpr2* and *Ide* belonging to the glucose metabolism with differential expression in a 6-month-old PP adult, did not show any significant difference between the clinical groups and controls (Fig. 7A and Suppl. Table 8). We next examined *Kcnj2* and *Egr2* which show downregulation in the PP model at 9 months (Table 2 and Fig. 5H) and observed high variability with no changes across stages (Suppl. Table 8 and Fig 7C). Among the cellular signaling genes, with specific repression in the PP model, we detect an opposite increasing trend in *c-Fos*, *c-Jun*, and *Notch1* to the PP model with a near to significant 3.1 upregulation of *c-Fos* in severe AD as compared to controls ($F_{2,21}$=3.2 p=0.061; Suppl. Table 8 and Fig 7D). In the lipid metabolism group, *Plin4* and *Lcn2* show no change opposite to the PP model (Suppl. Table 8 and Fig 7E), suggesting that those molecules are more implicated in vascular inflammation. To validate this assumption, we analyzed the vascular genes, *Klf4*, *Angptl4*, *Cyp1b1*, which showed transient alterations in the PP mode, and observed no change across stages (Suppl. Table 8 and Fig 7F). To understand the dependencies between the examined genes, we performed a correlation analysis using the aggregate population. In general, all interactions are moderately significant (r>0.5) with positive associations between *c-fos* and *GFAP,* matching the increasing trend of the two transcripts, which suggest a cell-type-specific change, while *c-fos* is negatively associated with *MAP2* (Fig. 7G). *Kcnj2* is inversely associated with *Ide* reflecting their opposite trend, while *Ide* is positively correlated with *Cyp1b1* (Fig. 7G), indicating potential dependencies. Other interactions among the studied genes are seen but too subtle to be of functional relevance. Overall,

despite the PolyI:C model replicates some aspects of the AD proteinopathy and microglia changes, the gene expression between the mouse and humans differs substantially, raising the possibility of a mixed-vascular-AD model with diverse genetic fingerprints.

Translation into vascular dementia

To verify the hypothesis of a mixed vascular-AD phenotype, we performed gene targets' validation on the second cohort of hippocampi from vascular dementia patients and age-matched healthy controls (Table 4 and Suppl. Table 2). Cell type-specific genes, *GFAP* and *Iba1*, indicate an increasing but not significant trend of microglia and astroglia, while MAP2 levels remain unchanged. Accordingly to our model, *Glpr2* decreases by 90% in vascular dementia as compared to controls ($F_{1,9}$=5.28 p=0.039; Fig. 7J and Suppl. Table 9) suggesting ongoing vascular hypoxia (Xie et al. 2018)). On the other hand, the inflammatory and vascular markers, *Lcn2* ($F_{1,9}$=4.96 p=0.05) and *Cyp1b1* ($F_{1,9}$=7.10 p=0.03) increase in vascular dementia as in the PP model (Fig. 7L and 7K and Suppl. Table 9). Opposite to the genetic expression in the mouse, *Klf4*, *Notch1* and *c-fos* levels rise in vascular dementia (Fig. 7M and 7Y and Suppl. Table 9). Correlation analysis of the differentially expressed genes in the aggregate cohort indicates a positive association (r>0.6) among *Lcn2, Notch1 and Klf4*, implicating those factors in the vascular pathology. Whereas, along the mechanistic trajectory of vascular remodeling a negative association is observed between *Glpr2* and the two angiogenesis genes, *Klf4* and *Cyp1b1*. These results indicate that a handful of the gene targets that are significantly affected upon systemic inflammation in the brain of PP mice are reproduced in vascular neurodegenerative dementia.

Discussion

Spread of peripheral inflammation to the brain

AD is a multifactorial complex disorder requiring the understanding of causal risk factors for proper treatment. Among those agents, microbial infections causing low-grade inflammatory responses over a lifetime are causally implicated in the development of AD with aging (Jamieson et al. 1991; Hammond et al. 2010; Miklossy et al. 2004; Readhead et al. 2018; Dominy et al. 2019). Experiments in transgenic mice for APP and Tau animals using viral and bacterial derivatives, such as PolyI:C and Lipopolysaccharides (LPS), aggravate the pathophysiological progression of AD (Krstic et al. 2012; Kitazawa et al. 2005). Based on these findings, we postulated that PolyI:C sterile infections prenatally and postnatally in young adulthood may be a sufficient driver of the AD-pathology as a result of sustained peripheral inflammation. Our cross-sectional and multi-modal examination of such an experimental model demonstrates that systemic infection with the double-stranded viral RNA surrogate, PolyI:C, causes the upregulation of circulating inflammatory humoral factors (MCP-1, IL-6, IL-10, and TNF-α) by 3 months of age which precedes the neuroinflammatory wave (IFN-γ, IL-6, IL-1β) occurring 3 months later. Despite no extravasation of neutrophils, monocytes nor polymorphonuclear cells to the brains at 3 and 6 months, supporting an intact blood-brain barrier at these stages, cytokines of the innate and adaptive immunity can spread from the periphery to the brain triggering deleterious neuroinflammatory events. This is

aligned with findings in humans where elevated IL-6 and IL-10 levels in the blood or brain of AD patients have been associated with the severity of cognitive decline and increased ventricular volume (Licastro et al. 2003; Leung et al. 2013). In parallel to the observed rise of neuroinflammation with aging, we also see an increase in microglia and astroglia gene expression at 6 and 9 months, reflecting cell-type-specific changes in these populations (Fig 1). Interestingly, in the very old animals at 16 months the inflammatory tone dissipates suggesting a late immune deficiency attributed to immunosenescence upon low-grade chronic inflammation typically of infectious origin (Pawelec et al. 2005; Furman et al. 2019).

Progressive proteinopathy

Along with rise in central inflammatory responses (IL-6 and IFN-γ), at 6 months of age PolyI:C brains display a rise in hippocampal tau phosphorylation supporting a causal link between IL-6 and tau hyperphosphorylation (p-Tau205/tau) as previously demonstrated in rat embryonic hippocampal neurons (Quintanilla 2004). At the same time soluble Aβ1-42 increases at 6 months, coinciding with the rise in neuroinflammation and the onset of the tauopathy. Recent reports have indicated that inflammatory cytokines can increase β-secretase activity in neurons, producing elevated Aβ1-42 (Alasmari et al. 2018; Hur et al. 2020), which is in line with our model. Furthermore, the notion that Aβ may be released as an antimicrobial agent against viral, bacterial or fungal infections (Soscia et al. 2010) supports the use of anti-inflammatory agents at the early stages as a preventive strategy to the proteinopathy (Hampel et al. 2020). In the aged PP mice, at 16 months, insoluble tangles or Aβ aggregates are visible in the hippocampus as small neuropil aggregates internalized at times by astroglia cells and in vessels reflecting a CAA. Interestingly, amyloid-β deposits in vessels are commonly seen in severe AD patients (53% of cases) but also in aged cognitively healthy individuals (50%) (Kövari et al. 2013). In old PP animals, amyloid-β fibrillary aggregates are observed clearly in the entorhinal cortex, likely contributing to its selective vulnerability (Stranahan and Mattson 2010) and the spatial reference memory deficit (Fyhn et al. 2004). Overall, the progressive proteinopathy as a result of chronic neuroinflammation disrupts neural networks' integrity affecting spatial memory encoding in PolyI:C mice and reproducing the topological pathogenesis in human AD (Heiko Braak et al. 2011; H. Braak and Braak 1996).

Microglia phenotypic change

Microglia are the major innate immune cells of the central nervous system mediating host defense responses against infectious agents, injury, abnormal accumulation of amyloid-β, and prion proteins (Yin et al. 2017). These cells express TLR3 viral receptors recognizing double-stranded RNA viruses (Town et al. 2006) and therefore play an important role in neuroinflammation in response to such stimuli initiating neuronal death. We have reported here a full-length characterization of microglial morphological changes across aging within the hippocampus of PolyI:C mice. We observe a typical pathological shift with aging from resting to ramified, rounded, and small soma to more hyper-ramified, reactive phagocytic morphology (Walkera, Nilsson, and Jones 2013). In alignment with our study, others have reported an enlargement in the microglia soma/volume and an increase in their branch points after bacterial LPS exposure (Siemsen et al. 2020). As proposed earlier (Knuesel et al. 2014), the dynamic changes in the

microglial morphology indicate a potential priming effect due to both maternal and early postnatal immune activation. In our study morphological changes in the aging PolyI:C mice resemble a microglial phenotype upon injury (Walker et al. 2014; Streit, Walter, and Pennell 1999) and after acute inflammatory response with neuraminidase treatment (Fernández-Arjona et al. 2017). Despite the recent evidence of a profoundly diverse genetic repertoire in rodents and human microglia (Masuda et al. 2019), the phenotypic transitions of microglia cells in this and other models recapitulate the dynamic undergoing changes in the progression of AD. Our and other findings support that neuroinflammation, passed on by the circulation and in response to the proteinopathy, is perpetuated influencing microglia cell fate to acquire a synapto- and neuro-toxic phenotype (Combs et al. 1999).

Genetic remodeling

To further support the use of the PolyI:C mouse model as a viable preclinical experimental animal for AD research, we discovered alterations in the hippocampal transcriptome relevant to synaptic dysfunction, inflammation and neurodegenerative dementia. GEA using the SynGO database indicates the biggest changes in presynaptic gene markers at the early stages (3 months), a steady state at 6 months, and from 9 months on a progressive enrichment in post-synaptic genes. This is in line with the observed early presynaptic release of glutamate in response to oligomeric Amyloid-β (Palop and Mucke 2010), followed in time by post-synaptic scaling events aimed at preserving neuronal integrity at the expense of synaptic transmission (Findley et al. 2019). This mechanistic progression is theoretically confirmed by an aggregate GEA using KEGG, Wikipathway and Reactome pathways, which shows an early abundance in calcium signaling cascades, inflammation pathways, including MAPK signaling, PI3K-AKT signaling associated to cell survival and apoptosis. While at 6 months we confirmed an important decrease in *Glpr2* associated to synaptic depotentiation in response to hyperactivity (Sasaki-Hamada, Ikeda, and Oka 2019), (Xie et al. 2018; Bhusal et al. 2019), genes associate to neuroinflammation such as *Lcn2* and *Plin4* were increased at the late stages. *Lcn2* is a key gene involved in iron regulation and inflammation (Dekens et al. 2018). Lcn2 in neurons and glial cells generates neuroinflammatory responses (Bi et al. 2013) associated with insulin resistance and synaptic modulation (Song and Kim 2018) whereas accumulation in the endothelial barrier affects BBB permeability (Ferreira et al. 2015). Lcn-2 is upregulated during systemic inflammation (Kang et al. 2017) and is elevated in the brains of AD patients (Naudé et al. 2012), suggesting that it may be a modifiable target in sporadic LOAD. On the other hand, *Plin4* is often associated with triacylglycerol metabolism and is involved in the biogenesis of lipid droplets in pathological degeneration (Han et al. 2018). The PolyI:C model shows a strong and specific rise in lipid droplets density accompanied by an increase in Lcn2 protein levels in neurons and glia, which confirms the metabolic and inflammatory imbalance. Interestingly, the origin of neurotoxic Lcn2 can be sourced back to astrocytes and increased levels of Lcn2 are seen in the brains of patients with human immunodeficiency virus 1 (HIV-1) reporting neurocognitive impairment (Ojeda-Juárez et al. 2020). Thus, Lcn-2 overexpression upon low-grade systemic inflammation supports its role as a putative druggable target to halt the immune-driven neuropathological progression.

Reproducibility in postmortem tissue from AD and vascular dementia patients

One of the challenges of understanding the physiopathology of AD to develop targetable therapeutics is partially attributed to the poor reproducibility between animal models and humans and multifactorial etiology of the disease (Götz, Bodea, and Goedert 2018). Inflammatory, vascular processes and misfolded proteins should be considered as a whole and investigated closely to unravel dependencies. Furthermore, overlapping pathologies between AD and VaD, representing over 20% of the cases supporting common mechanisms and therapeutic investigations. Consistently, our study indicates that the PP model shows an AD proteinopathy coupled with a vascular deficit. This conclusion derives from our DEG target repertoire analysis in two cohorts representing i) progressive AD stages and ii) vascular dementia. We confirm an astrogliosis in AD, captured by increased GFAP levels, comparable to the PP model. While this effect is present it is less pronounced in VaD. Interestingly, astrogliosis has been shown to increase proportionally to the extent of cognitive decline and is strongly associated with plaques and tangle formation (Serrano-Pozo et al. 2011). On the other hand, in VaD, astrogliosis and astroglial endfeet swelling has been implicated as one of the triggering factors for vascular damage (Price et al. 2018; Wang et al. 2018). In both instances, reactive astrogliosis is a commonality of the two diseases associated with the production of pro-inflammatory cytokines. Along with the increase in *GFAP* expression, we see a positive association with *c-fos* and *Notch1* levels in the severe AD stage, supporting the proliferation of astroglia (Hisanaga et al. 1990) and the role of Notch1 in driving astroglia proliferation in response to inflammation through the proto-oncogene *c-fos* (Acaz-Fonseca et al. 2019). This data is in opposition to the PP mouse model, where despite an increase in astroglia, a decline in *c-fos* and *Notch1* is observed at 9 months. The discrepancy can be explained by the different signaling profiles of glia and neurons in rodents, suggesting that cellular cascades may be cell-specific depending on the species.

Investigating the genes involved in mediating vascular function (Deniz, Bozkurt, and Kurtel 2007), we observe no change in *Glpr2* expression in the progression of AD, while in VaD, *Glpr2* is downregulated similarly to the PP model supporting that cognitive deficit is contributed by lower blood perfusion (Xie et al. 2018). Along the same lines, the progressive increase in the inflammatory and metabolic markers, *Lcn2*, displayed by aging PP animals, is not reproduced in AD but in the VaD specimen. This finding is in contrast to the previous reports of a rise in Lcn2 protein levels in the hippocampus of severe AD subjects (Naudé et al. 2012) and patients with MCI (Choi, Lee, and Suk 2011), but is completely aligned with the recently reported upregulation of Lcn2 in CSF from VaD (n.d.; Llorens et al. 2020b). In support of the microvessel damage mediated by Lcn2 (J.-H. Kim et al. 2017), 9 months old PP mice report a rise in *Cyp1b1*, *Angptl4* and reduction in Klf4, which all regulate the BB permeability (Sangwung et al. 2017; Palenski et al. 2013; Huang et al. 2011). While, in AD, those markers remain unchanged, in VaD *Cyp1b1* is increased together with *Klf4*, while *Angptl4* remains unchanged. The different directionality of those vascular markers between mouse and human can be explained either by the time point of sampling or the species diversity. Nevertheless, a vascular pathology in the PP model is supported by a two-fold reduction of Claudin 5, *Cldn5*, a key regulator of BBB permeability. The rise in proinflammatory cytokines causes disruption of BBB's tight junction and endothelial proteins like Cldn5 and vascular angiogenic factors like Angptl4 which has been largely identified in various neuroinflammatory and neuroinfectious diseases

caused by RNA viruses (Bertrand, Velichkovska, and Toborek 2019; Salimi and Klein 2019; Liu et al. 2019; Leda et al. 2019). While the number of human samples analyzed is small, the translational validation of the PolyI:C data clearly demonstrates that this mouse model can reproduce some of the characteristic features of reactive central inflammation (Hampel et al. 2020) and vascular pathology encountered in neurodegenerative dementia.

Conclusion

Overall, the present research, using a redesigned PolyI:C mouse model of sterile infection (Kristic et al. 2012), demonstrates that chronic systemic inflammation during adulthood causes progressive neuropathology with neuroinflammation, insoluble protein aggregates, vascular permeability, microglia remodeling and behavioral deficits, mimicking a mixed vascular-AD pathology. Although AD pre-clinical animal models are useful, one should acknowledge the limitations they possess in exhibiting the complete pathology, complex and diverse etiology seen in AD, particularly when it comes to shared mixed vascular-AD. Our post-mortem analysis on AD and VaD brain specimens shows partially overlapping genetic profiles between VaD and the PolyI:C mouse, which emphasizes the effect of systemic inflammation in causing vascular deficit besides neuroinflammation and the proteinopathy. Indeed, chronic inflammation is known to pose a risk for cardiovascular health which with aging may contribute to overlapping pathologies (Metti and Cauley 2012; Newcombe et al. 2018). This is further supported by recent evidence indicating that hyperphosphorylated Tau can cause neurovascular decoupling (Park et al. 2020) bridging characteristic AD-mechanisms to vascular deficits. Another important limitation of the current study is that we have not examined such anatomical or biochemical differences by sex as only male animals were included in this study. However, AD pathological hallmarks remain largely the same between both the sexes (Yanguas-Casás 2020). Also, the precise mechanisms through which PolyI:C induces inflammation is inferred but not tested at this instance. Although a translational attempt has been made by validating selected transcriptional targets in AD and VaD brain specimens, the sample size is low, limiting its analytical power. Nevertheless, our large descriptive study provides insights into the role of systemic and CNS inflammation in mixed AD pathologies, which are particularly important considering the long-term effects of neurotropic viral infections. The study is of use not only for the understanding of the interplay between peripheral and central processes but also presents a surrogate animal model displaying a sporadic vascular AD-mixed phenotype, which can be used for testing therapeutics against pathological brain aging.

List Of Abbreviations

ABCA7	ATP-binding cassette sub-family A member 7
AD	Alzheimer’s disease
Angptl4	Angiopoietin like 4

ApoE	Apolipoprotein E
ApoEε4	Apolipoprotein E variant ε4
Aβ	Amyloid beta
BBB	Blood Brain Barrier
BIN1	Box-dependent-interacting protein 1
CA	Cornu Ammonis
CAA	Cerebral Amyloid Angiopathy
CD2AP	CD2 Associated Protein
CD33	Myeloid Cell Surface Antigen CD3
CELF1	CUGBP Elav-like family member 1
c-fos	Proto-oncogene c-Fos
Cyp1b1	Cytochrome P450 1B1
Cldn5	Claudin 5
CLU	Clusterin
CNS	Central Nervous System
CR1	Complement receptor type 1
CSF	Cerebrospinal fluid
CTL	Control
Cx	Cortex
DABCO	1,4-diazabicyclo [2.2.2] octane
DAPI	4',6-diamidino-2-phenylindole
DEGs	Differentially Expressed Genes
dsRNA	Double-strand RNA
EC	Entorhinal cortex

EDTA	Ethylenediaminetetraacetic acid
EGR2	Early growth response protein 2
EPHA1	Ephrin type-A receptor 1
FERMT2	Fermitin family homolog 2
GD	Gestational Day
GEA	Gene enrichment analysis
GFAP	Glial fibrillary acidic protein
GLPR2	Glucagon like peptide 2 receptor
GO	Gene ontology
GRIN1	Glutamate Ionotropic Receptor NMDA Type Subunit 1
GWAS	Genome Wide Association Studies
H2-Aa	H-2 class II histocompatibility antigen, A-B alpha chain
Iba-1	Ionized calcium binding adaptor molecule1
Ide	Insulin degrading enzyme
IL	Interleukin
INPP5D	Phosphatidylinositol 3,4,5-trisphosphate 5-phosphatase 1
KCNJ2	Potassium Inwardly Rectifying Channel Subfamily J Member 2
KEGG	Kyoto Encyclopedia of Genes and Genomes
Klf4	zinc finger-containing Krüppel-like factor
KS	Kolmogorov-Smirnov
c-Jun	Transcription factor AP-1
LCN2	Lipocalin 2
LOAD	Late-onset AD
LPS	Lipopolysaccharide

MAP2	Microtubule-associated protein 2
MAPK	Mitogen-activated protein kinase 1
MCI	Mild Cognitive Impairment
MCP-1	Monocyte Chemoattractant Protein-1
MEF2C	Myocyte-specific enhancer factor 2C
mM	milliMolar
M-MLV	Moloney Murine Leukemia Virus Reverse Transcriptase
mo	month
mRNA	Messenger RNA
MS4A4A	Membrane-spanning 4-domains subfamily A member 4A
ND	Neurodegenerative disease
NME8	Thioredoxin domain-containing protein 3
NN	Saline controls
Notch1	Neurogenic locus notch homolog protein 1
PFA	Paraformaldehyde
PICALM	Phosphatidylinositol-binding clathrin assembly protein
PLCG2	1-phosphatidylinositol 4,5-bisphosphate phosphodiesterase gamma-2
pM	picomolar
PLIN4	Perilipin 4
PMNs	Polymorphonuclear neutrophils
PolyI:C	Polyinosinic:Polycytidylic acid
PSEN	Presenilin
PP	PolyI:C injected animals
pTau	Phosphorylated tau

PVA	Polyvinyl alcohol
rpm	revolutions per minute
rRNA	ribosomal RNA
r	Spearman's Rank Correlation
SEM	Standard Error Mean
SLC24A4	Sodium/potassium/calcium exchanger 4
SORL1	Sortilin-related receptor
SRCAP	Snf2-related CREBBP activator protein
TBS	Trizma-based salt solution
TLRs	Toll Like receptors
TNFα	Tumor necrosis factor alpha
TREM2	Triggering receptor expressed on myeloid cells 2
ZCWPW1	Zinc finger CW-type PWWP domain protein 1
µg	microgram
µm	micrometer

Declarations

Ethics Approval and Consent to participate

Animal experimentation was approved by the animal experiment committee, University of Fribourg (Protocol no. 2016_32_FR registered 01/01/2017).

The use of human tissue has been approved by the Ethical Commission of the Brain Bank for Dementia UK (OBB443 registered 1/05/2017 and OB344 registered 1/02/2014), Stanford (Stanford IRB), and the Ethical Commission from the Canton of Fribourg and Vaud (N. 325/14). All experiments conducted on human tissue comply with the WMA Declaration of Helsinki.

Consent for publication

All authors agree on publishing the original data

Availability of data and materials

Supporting data is available in the form of supplementary material and tables. All raw data is available on request.

Competing interests

There are no competing interests

Funding

Schweizerischer Nationalfonds zur Förderung der Wissenschaftlichen Forschung (163470)(LA). Bundesbehörden der Schweizerischen Eidgenossenschaft (2017.0480) (PB).

Authors' contributions

PB conducted the main bulk of the experiments and contributed to the writing. ID performed the bioinformatic analysis. EZ and ET performed the cellular immunology experiments from blood and brain. AF and EB performed the blind quantitative analysis of microglia morphology using custom-made scripts. MAD assisted in the inflammatory model characterization. LA designed the study and wrote the manuscript. All authors read and approved the final manuscript

Acknowledgements

We would like to thank Mrs. E. Martin and V. Tache for the technical support. We are also grateful to Dr. M. Reggente in providing his expertise in R. We thank Prof. T. Montine for sharing the brain tissue from the Stanford Biobank for this study. We are thankful to the donors and their families for allowing us access to the human tissue (Oxford, UK and Stanford, USA).

References

Acaz-Fonseca, Estefania, Ana Ortiz-Rodriguez, Iñigo Azcoitia, Luis M. Garcia-Segura, and Maria-Angeles Arevalo. 2019. “Notch Signaling in Astrocytes Mediates Their Morphological Response to an Inflammatory Challenge.” *Cell Death Discovery* 5 (April): 85.

Alasmari, Fawaz, Musaad A. Alshammari, Abdullah F. Alasmari, Wael A. Alanazi, and Khalid Alhazzani. 2018. “Neuroinflammatory Cytokines Induce Amyloid Beta Neurotoxicity through Modulating Amyloid Precursor Protein Levels/Metabolism.” *BioMed Research International* 2018 (October): 3087475.

Barber, Robert C. 2012. “The Genetics of Alzheimer’s Disease.” *Scientifica* 2012 (December). https://doi.org/10.6064/2012/246210.

Bertrand, Luc, Martina Velichkovska, and Michal Toborek. 2019. “Cerebral Vascular Toxicity of Antiretroviral Therapy.” *Journal of Neuroimmune Pharmacology: The Official Journal of the Society on NeuroImmune Pharmacology*, June. https://doi.org/10.1007/s11481-019-09858-x.

Bhusal, Anup, Md Habibur Rahman, In-Kyu Lee, and Kyoungho Suk. 2019. “Role of Hippocampal Lipocalin-2 in Experimental Diabetic Encephalopathy.” *Frontiers in Endocrinology* 10. https://doi.org/10.3389/fendo.2019.00025.

Bi, Fangfang, Cao Huang, Jianbin Tong, Guang Qiu, Bo Huang, Qinxue Wu, Fang Li, et al. 2013. “Reactive Astrocytes Secrete lcn2 to Promote Neuron Death.” *Proceedings of the National Academy of Sciences of the United States of America* 110 (10): 4069–74.

Bilbo, Staci D., Carina L. Block, Jessica L. Bolton, Richa Hanamsagar, and Phuong K. Tran. 2018. “Beyond Infection - Maternal Immune Activation by Environmental Factors, Microglial Development, and Relevance for Autism Spectrum Disorders.” *Experimental Neurology* 299 (Pt A): 241–51.

Binda, Anna, Ilaria Rivolta, Chiara Villa, Elisa Chisci, Massimiliano Beghi, Cesare M. Cornaggia, Roberto Giovannoni, and Romina Combi. 2018. “A Novel KCNJ2 Mutation Identified in an Autistic Proband Affects the Single Channel Properties of Kir2.1.” *Frontiers in Cellular Neuroscience*. https://doi.org/10.3389/fncel.2018.00076.

Bindea, Gabriela, Bernhard Mlecnik, Hubert Hackl, Pornpimol Charoentong, Marie Tosolini, Amos Kirilovsky, Wolf-Herman Fridman, Franck Pagès, Zlatko Trajanoski, and Jérôme Galon. 2009. “ClueGO: A Cytoscape Plug-in to Decipher Functionally Grouped Gene Ontology and Pathway Annotation Networks.” *Bioinformatics* 25 (8): 1091–93.

Braak, H., and E. Braak. 1996. “Evolution of the Neuropathology of Alzheimer’s Disease.” *Acta Neurologica Scandinavica. Supplementum* 165: 3–12.

Braak, Heiko, Dietmar R. Thal, Estifanos Ghebremedhin, and Kelly Del Tredici. 2011. “Stages of the Pathologic Process in Alzheimer Disease: Age Categories from 1 to 100 Years.” *Journal of Neuropathology and Experimental Neurology* 70 (11): 960–69.

Brai, Emanuele, and Lavinia Alberi. 2015. “Simple and Computer-Assisted Olfactory Testing for Mice.” *Journal of Visualized Experiments: JoVE*, no. 100 (June): e52944.

Brai, Emanuele, Swananda Marathe, Simone Astori, Naila Ben Fredj, Elisabeth Perry, Christophe Lamy, Alessandra Scotti, and Lavinia Alberi. 2015. “Notch1 Regulates Hippocampal Plasticity Through Interaction with the Reelin Pathway, Glutamatergic Transmission and CREB Signaling.” *Frontiers in Cellular Neuroscience* 9 (November): 447.

Carvey, Paul M., Qin Chang, Jack W. Lipton, and Zaodung Ling. 2003. “Prenatal Exposure to the Bacteriotoxin Lipopolysaccharide Leads to Long-Term Losses of Dopamine Neurons in Offspring: A Potential, New Model of Parkinson’s Disease.” *Frontiers in Bioscience: A Journal and Virtual Library* 8 (September): s826–37.

Chakraborty, Ananya, Alwin Kamermans, Bert van het Hof, Kitty Castricum, Ed Aanhane, Jack van Horssen, Victor L. Thijssen, et al. 2018. “Angiopoietin like-4 as a Novel Vascular Mediator in Capillary Cerebral Amyloid Angiopathy.” *Brain*. https://doi.org/10.1093/brain/awy274.

Choi, Jihye, Ho-Won Lee, and Kyoungho Suk. 2011. “Increased Plasma Levels of Lipocalin 2 in Mild Cognitive Impairment.” *Journal of the Neurological Sciences* 305 (1-2): 28–33.

Combs, Colin K., Derrick E. Johnson, Steve B. Cannady, Timothy M. Lehman, and Gary E. Landreth. 1999. “Identification of Microglial Signal Transduction Pathways Mediating a Neurotoxic Response to Amyloidogenic Fragments of β-Amyloid and Prion Proteins.” *The Journal of Neuroscience: The Official Journal of the Society for Neuroscience* 19 (3): 928–39.

Conway, Fiona, and Alan S. Brown. 2019. “Maternal Immune Activation and Related Factors in the Risk of Offspring Psychiatric Disorders.” *Frontiers in Psychiatry / Frontiers Research Foundation* 10 (June): 430.

Crawley, Jacqueline, and Kathleen Bailey. 2008. “Anxiety-Related Behaviors in Mice.” *Methods of Behavior Analysis in Neuroscience, Second Edition*. https://doi.org/10.1201/noe1420052343.ch5.

Cunningham, Colm. 2013. “Microglia and Neurodegeneration: The Role of Systemic Inflammation.” *Glia* 61 (1): 71–90.

Cunningham, Colm, and Edel Hennessy. 2015. “Co-Morbidity and Systemic Inflammation as Drivers of Cognitive Decline: New Experimental Models Adopting a Broader Paradigm in Dementia Research.” *Alzheimer’s Research & Therapy* 7 (1): 1–13.

Davis, Benjamin M., Manual Salinas-Navarro, M. Francesca Cordeiro, Lieve Moons, and Lies De Groef. 2017. “Characterizing Microglia Activation: A Spatial Statistics Approach to Maximize Information Extraction.” *Scientific Reports* 7 (1): 1576.

De Chiara, Giovanna, Roberto Piacentini, Marco Fabiani, Alessia Mastrodonato, Maria Elena Marcocci, Dolores Limongi, Giorgia Napoletani, et al. 2019. “Recurrent Herpes Simplex Virus-1 Infection Induces Hallmarks of Neurodegeneration and Cognitive Deficits in Mice.” *PLoS Pathogens* 15 (3): e1007617.

Dekens, Doortje W., Peter P. De Deyn, Friederike Sap, Ulrich L. M. Eisel, and Petrus J. W. Naudé. 2020. “Iron Chelators Inhibit Amyloid-β-Induced Production of Lipocalin 2 in Cultured Astrocytes.” *Neurochemistry International* 132 (January): 104607.

Dekens, Doortje W., Petrus J. W. Naudé, Jan N. Keijser, Ate S. Boerema, Peter P. De Deyn, and Ulrich L. M. Eisel. 2018. “Lipocalin 2 Contributes to Brain Iron Dysregulation but Does Not Affect Cognition, Plaque Load, and Glial Activation in the J20 Alzheimer Mouse Model.” *Journal of Neuroinflammation* 15 (1): 330.

Deniz, Mustafa, Ayhan Bozkurt, and Hizir Kurtel. 2007. “Mediators of Glucagon-like Peptide 2-Induced Blood Flow: Responses in Different Vascular Sites.” *Regulatory Peptides* 142 (1-2): 7–15.

Dominy, Stephen S., Casey Lynch, Florian Ermini, Malgorzata Benedyk, Agata Marczyk, Andrei Konradi, Mai Nguyen, et al. 2019. “Porphyromonas Gingivalis in Alzheimer’s Disease Brains: Evidence for Disease Causation and Treatment with Small-Molecule Inhibitors.” *Science Advances* 5 (1): eaau3333.

Du, Yanjiao, Chao Liu, Congmin Ma, Xiaohui Xu, Xufeng Zhou, Haitao Zhou, and Chao Huang. 2019. “Cerebral Amyloid Angiopathy-Related Inflammation: A Case Report Presenting with a Rare Variant in SORL1 Gene.” *BMC Neurology* 19 (1): 97.

Engelhart, Marianne J., Mirjam I. Geerlings, John Meijer, Amanda Kiliaan, Annemieke Ruitenberg, John C. van Swieten, Theo Stijnen, Albert Hofman, Jacqueline C. M. Witteman, and Monique M. B. Breteler. 2004. “Inflammatory Proteins in Plasma and the Risk of Dementia: The Rotterdam Study.” *Archives of Neurology* 61 (5): 668–72.

Fernández-Arjona, María del Mar, María del Mar Fernández-Arjona, Jesús M. Grondona, Pablo Granados-Durán, Pedro Fernández-Llebrez, and María D. López-Ávalos. 2017. “Microglia Morphological Categorization in a Rat Model of Neuroinflammation by Hierarchical Cluster and Principal Components Analysis.” *Frontiers in Cellular Neuroscience*. https://doi.org/10.3389/fncel.2017.00235.

Ferreira, Ana C., Sandro Dá Mesquita, João C. Sousa, Margarida Correia-Neves, Nuno Sousa, Joana A. Palha, and Fernanda Marques. 2015. “From the Periphery to the Brain: Lipocalin-2, a Friend or Foe?” *Progress in Neurobiology*. https://doi.org/10.1016/j.pneurobio.2015.06.005.

Findley, Caleigh A., Andrzej Bartke, Kevin N. Hascup, and Erin R. Hascup. 2019. “Amyloid Beta-Related Alterations to Glutamate Signaling Dynamics During Alzheimer’s Disease Progression.” *ASN Neuro*. https://doi.org/10.1177/1759091419855541.

Fulop, Tamas, Jacek M. Witkowski, Karine Bourgade, Abdelouahed Khalil, Echarki Zerif, Anis Larbi, Katsuiku Hirokawa, et al. 2018. “Can an Infection Hypothesis Explain the Beta Amyloid Hypothesis of Alzheimer’s Disease?” *Frontiers in Aging Neuroscience* 10 (July): 224.

Furman, David, Judith Campisi, Eric Verdin, Pedro Carrera-Bastos, Sasha Targ, Claudio Franceschi, Luigi Ferrucci, et al. 2019. “Chronic Inflammation in the Etiology of Disease across the Life Span.” *Nature Medicine* 25 (12): 1822–32.

Fyhn, Marianne, Sturla Molden, Menno P. Witter, Edvard I. Moser, and May-Britt Moser. 2004. “Spatial Representation in the Entorhinal Cortex.” *Science* 305 (5688): 1258–64.

Ghosh, Chaitali, Mohammed Hossain, Jesal Solanki, Aaron Dadas, Nicola Marchi, and Damir Janigro. 2016. “Pathophysiological Implications of Neurovascular P450 in Brain Disorders.” *Drug Discovery Today*. https://doi.org/10.1016/j.drudis.2016.06.004.

Giovanoli, Sandra, Tina Notter, Juliet Richetto, Marie A. Labouesse, Stéphanie Vuillermot, Marco A. Riva, and Urs Meyer. 2015. “Late Prenatal Immune Activation Causes Hippocampal Deficits in the Absence of

Persistent Inflammation across Aging." *Journal of Neuroinflammation* 12 (November): 221.

Götz, Jürgen, Liviu-Gabriel Bodea, and Michel Goedert. 2018. "Rodent Models for Alzheimer Disease." *Nature Reviews. Neuroscience* 19 (10): 583–98.

Greenspan, P., E. P. Mayer, and S. D. Fowler. 1985. "Nile Red: A Selective Fluorescent Stain for Intracellular Lipid Droplets." *The Journal of Cell Biology* 100 (3): 965–73.

Hammond, Christine J., Loretta R. Hallock, Raymond J. Howanski, Denah M. Appelt, C. Scott Little, and Brian J. Balin. 2010. "Immunohistological Detection of Chlamydia Pneumoniae in the Alzheimer's Disease Brain." *BMC Neuroscience* 11 (September): 121.

Hampel, Harald, Filippo Caraci, A. Claudio Cuello, Giuseppe Caruso, Robert Nisticò, Massimo Corbo, Filippo Baldacci, et al. 2020. "A Path Toward Precision Medicine for Neuroinflammatory Mechanisms in Alzheimer's Disease." *Frontiers in Immunology* 11 (March): 456.

Han, Xiaojuan, Jialei Zhu, Xinlei Zhang, Qiqi Song, Jianhua Ding, Ming Lu, Sifan Sun, and Gang Hu. 2018. "Plin4-Dependent Lipid Droplets Hamper Neuronal Mitophagy in the MPTP/p-Induced Mouse Model of Parkinson's Disease." *Frontiers in Neuroscience*. https://doi.org/10.3389/fnins.2018.00397.

Hisanaga, K., S. M. Sagar, K. J. Hicks, R. A. Swanson, and F. R. Sharp. 1990. "C-Fos Proto-Oncogene Expression in Astrocytes Associated with Differentiation or Proliferation but Not Depolarization." *Brain Research. Molecular Brain Research* 8 (1): 69–75.

Hoeijmakers, Lianne, Yvonne Heinen, Anne-Marie van Dam, Paul J. Lucassen, and Aniko Korosi. 2016. "Microglial Priming and Alzheimer's Disease: A Possible Role for (Early) Immune Challenges and Epigenetics?" *Frontiers in Human Neuroscience*. https://doi.org/10.3389/fnhum.2016.00398.

Huang, Royston-Luke, Ziqiang Teo, Han Chung Chong, Pengcheng Zhu, Ming Jie Tan, Chek Kun Tan, Chee Ren Ivan Lam, et al. 2011. "ANGPTL4 Modulates Vascular Junction Integrity by Integrin Signaling and Disruption of Intercellular VE-Cadherin and Claudin-5 Clusters." *Blood* 118 (14): 3990–4002.

Hui, Chin W., Abygaël St-Pierre, Hassan El Hajj, Yvan Remy, Sébastien S. Hébert, Giamal N. Luheshi, Lalit K. Srivastava, and Marie-Ève Tremblay. 2018. "Prenatal Immune Challenge in Mice Leads to Partly Sex-Dependent Behavioral, Microglial, and Molecular Abnormalities Associated with Schizophrenia." *Frontiers in Molecular Neuroscience* 11 (February): 13.

Hur, Ji-Yeun, Georgia R. Frost, Xianzhong Wu, Christina Crump, Si Jia Pan, Eitan Wong, Marilia Barros, et al. 2020. "The Innate Immunity Protein IFITM3 Modulates γ-Secretase in Alzheimer's Disease." *Nature*, September. https://doi.org/10.1038/s41586-020-2681-2.

Ito, Hiroshi T., Stephen E. P. Smith, Elaine Hsiao, and Paul H. Patterson. 2010. "Maternal Immune Activation Alters Nonspatial Information Processing in the Hippocampus of the Adult Offspring." *Brain, Behavior, and Immunity* 24 (6): 930–41.

Itzhaki, Ruth F., and Matthew A. Wozniak. 2006. “Herpes Simplex Virus Type 1, Apolipoprotein E, and Cholesterol: A Dangerous Liaison in Alzheimer’s Disease and Other Disorders.” *Progress in Lipid Research* 45 (1): 73–90.

Jamieson, G. A., N. J. Maitland, G. K. Wilcock, J. Craske, and R. F. Itzhaki. 1991. “Latent Herpes Simplex Virus Type 1 in Normal and Alzheimer’s Disease Brains.” *Journal of Medical Virology* 33 (4): 224–27.

Jha, Mithilesh Kumar, Shinrye Lee, Dong Ho Park, Hyun Kook, Keun-Gyu Park, In-Kyu Lee, and Kyoungho Suk. 2015. “Diverse Functional Roles of Lipocalin-2 in the Central Nervous System.” *Neuroscience and Biobehavioral Reviews* 49 (February): 135–56.

Kang, S. S., Y. Ren, C-C Liu, A. Kurti, K. E. Baker, G. Bu, Y. Asmann, and J. D. Fryer. 2017. “Lipocalin-2 Protects the Brain during Inflammatory Conditions.” *Molecular Psychiatry* 23 (2): 344–50.

Kim, Eun Kyung, and Eui-Ju Choi. 2010. “Pathological Roles of MAPK Signaling Pathways in Human Diseases.” *Biochimica et Biophysica Acta* 1802 (4): 396–405.

Kim, Jae-Hong, Pan-Woo Ko, Ho-Won Lee, Ji-Young Jeong, Maan-Gee Lee, Jong-Heon Kim, Won-Ha Lee, Ri Yu, Won-Jong Oh, and Kyoungho Suk. 2017. “Astrocyte-Derived Lipocalin-2 Mediates Hippocampal Damage and Cognitive Deficits in Experimental Models of Vascular Dementia.” *Glia* 65 (9): 1471–90.

Kinney, Jefferson W., Shane M. Bemiller, Andrew S. Murtishaw, Amanda M. Leisgang, Arnold M. Salazar, and Bruce T. Lamb. 2018. “Inflammation as a Central Mechanism in Alzheimer’s Disease.” *Alzheimer’s & Dementia : Translational Research & Clinical Interventions* 4: 575.

Kitazawa, Masashi, Salvatore Oddo, Tritia R. Yamasaki, Kim N. Green, and Frank M. LaFerla. 2005. “Lipopolysaccharide-Induced Inflammation Exacerbates Tau Pathology by a Cyclin-Dependent Kinase 5-Mediated Pathway in a Transgenic Model of Alzheimer’s Disease.” *The Journal of Neuroscience: The Official Journal of the Society for Neuroscience* 25 (39): 8843–53.

Knuesel, Irene, Laurie Chicha, Markus Britschgi, Scott A. Schobel, Michael Bodmer, Jessica A. Hellings, Stephen Toovey, and Eric P. Prinssen. 2014. “Maternal Immune Activation and Abnormal Brain Development across CNS Disorders.” *Nature Reviews. Neurology* 10 (11): 643–60.

Koopmans, Frank, Pim van Nierop, Maria Andres-Alonso, Andrea Byrnes, Tony Cijsouw, Marcelo P. Coba, L. Niels Cornelisse, et al. 2019. “SynGO: An Evidence-Based, Expert-Curated Knowledge Base for the Synapse.” *Neuron* 103 (2): 217–34.e4.

Kövari, E., F. R. Herrmann, P. R. Hof, and C. Bouras. 2013. “The Relationship between Cerebral Amyloid Angiopathy and Cortical Microinfarcts in Brain Ageing and Alzheimer’s Disease.” *Neuropathology and Applied Neurobiology* 39 (5): 498–509.

Krstic, Dimitrije, Amrita Madhusudan, Jana Doehner, Prisca Vogel, Tina Notter, Claudine Imhof, Abigail Manalastas, et al. 2012. “Systemic Immune Challenges Trigger and Drive Alzheimer-like Neuropathology

in Mice." *Journal of Neuroinflammation* 9 (July): 151.

Leda, Ana Rachel, Luc Bertrand, Ibolya Edit Andras, Nazira El-Hage, Madhavan Nair, and Michal Toborek. 2019. "Selective Disruption of the Blood–Brain Barrier by Zika Virus." *Frontiers in Microbiology*. https://doi.org/10.3389/fmicb.2019.02158.

Leung, Rufina, Petroula Proitsi, Andrew Simmons, Katie Lunnon, Andreas Güntert, Deborah Kronenberg, Megan Pritchard, et al. 2013. "Inflammatory Proteins in Plasma Are Associated with Severity of Alzheimer's Disease." *PloS One* 8 (6): e64971.

Licastro, Federico, Luigi Maria Edoardo Grimaldi, Massimiliano Bonafè, Chiappelli Martina, Fabiola Olivieri, Luca Cavallone, Simona Giovanietti, Eliezer Masliah, and Claudio Franceschi. 2003. "Interleukin-6 Gene Alleles Affect the Risk of Alzheimer's Disease and Levels of the Cytokine in Blood and Brain." *Neurobiology of Aging* 24 (7): 921–26.

Li, Jun-Wei, Yu Zong, Xi-Peng Cao, Lin Tan, and Lan Tan. 2018. "Microglial Priming in Alzheimer's Disease." *Annals of Translational Medicine* 6 (10): 176.

Linard, Morgane, Luc Letenneur, Isabelle Garrigue, Angélique Doize, Jean-François Dartigues, and Catherine Helmer. 2020. "Interaction between APOE4 and Herpes Simplex Virus Type 1 in Alzheimer's Disease." *Alzheimer's & Dementia: The Journal of the Alzheimer's Association* 16 (1): 200–208.

Ling, E. A., and W. C. Wong. 1993. "The Origin and Nature of Ramified and Amoeboid Microglia: A Historical Review and Current Concepts." *Glia* 7 (1): 9–18.

Lin, Yen-Feng, Albert Vernon Smith, Thor Aspelund, Rebecca A. Betensky, Jordan W. Smoller, Vilmundur Gudnason, Lenore J. Launer, and Deborah Blacker. 2019. "Genetic Overlap between Vascular Pathologies and Alzheimer's Dementia and Potential Causal Mechanisms." *Alzheimer's & Dementia: The Journal of the Alzheimer's Association* 15 (1): 65–75.

Little, C. Scott, Christine J. Hammond, Angela MacIntyre, Brian J. Balin, and Denah M. Appelt. 2004. "Chlamydia Pneumoniae Induces Alzheimer-like Amyloid Plaques in Brains of BALB/c Mice." *Neurobiology of Aging* 25 (4): 419–29.

Liu, Lu, Jixuan Li, Dong Huo, Zhong Peng, Ruicheng Yang, Jiyang Fu, Bojie Xu, Bo Yang, Huanchun Chen, and Xiangru Wang. 2019. "Meningitic Escherichia Coli Induction of ANGPTL4 in Brain Microvascular Endothelial Cells Contributes to Blood-Brain Barrier Disruption via ARHGAP5/RhoA/MYL5 Signaling Cascade." *Pathogens* 8 (4). https://doi.org/10.3390/pathogens8040254.

Llorens, Franc, Peter Hermann, Anna Villar-Piqué, Daniela Diaz-Lucena, Katarina Nägga, Oskar Hansson, Isabel Santana, et al. 2020a. "Cerebrospinal Fluid Lipocalin 2 as a Novel Biomarker for the Differential Diagnosis of Vascular Dementia." *Nature Communications* 11 (1): 619.

———. 2020b. “Cerebrospinal Fluid Lipocalin 2 as a Novel Biomarker for the Differential Diagnosis of Vascular Dementia.” *Nature Communications* 11 (1): 619.

Masuda, Takahiro, Roman Sankowski, Ori Staszewski, Chotima Böttcher, Lukas Amann, Sagar, Christian Scheiwe, et al. 2019. “Spatial and Temporal Heterogeneity of Mouse and Human Microglia at Single-Cell Resolution.” *Nature* 566 (7744): 388–92.

McHugh, Stephen B., Burkhard Niewoehner, J. N. P. Rawlins, and David M. Bannerman. 2008. “Dorsal Hippocampal N-Methyl-D-Aspartate Receptors Underlie Spatial Working Memory Performance during Non-Matching to Place Testing on the T-Maze.” *Behavioural Brain Research* 186 (1): 41–47.

Metti, Andrea L., and Jane A. Cauley. 2012. “How Predictive of Dementia Are Peripheral Inflammatory Markers in the Elderly?” *Neurodegenerative Disease Management* 2 (6): 609–22.

Miedel, Christian J., Jennifer M. Patton, Andrew N. Miedel, Edward S. Miedel, and Jonathan M. Levenson. 2017. “Assessment of Spontaneous Alternation, Novel Object Recognition and Limb Clasping in Transgenic Mouse Models of Amyloid-β and Tau Neuropathology.” *Journal of Visualized Experiments: JoVE*, no. 123 (May). https://doi.org/10.3791/55523.

Miklossy, Judith, Kamel Khalili, Lise Gern, Rebecca L. Ericson, Pushpa Darekar, Lorie Bolle, Jean Hurlimann, and Bruce J. Paster. 2004. “Borrelia Burgdorferi Persists in the Brain in Chronic Lyme Neuroborreliosis and May Be Associated with Alzheimer Disease.” *Journal of Alzheimer’s Disease: JAD* 6 (6): 639–49; discussion 673–81.

Morgan, Angharad R., Samuel Touchard, Claire Leckey, Caroline O’Hagan, Alejo J. Nevado-Holgado, NIMA Consortium, Frederik Barkhof, et al. 2019. “Inflammatory Biomarkers in Alzheimer’s Disease Plasma.” *Alzheimer’s & Dementia: The Journal of the Alzheimer's Association* 15 (6): 776–87.

Naudé, Petrus J. W., Csaba Nyakas, Lee E. Eiden, Djida Ait-Ali, Ragna van der Heide, Sebastiaan Engelborghs, Paul G. M. Luiten, Peter P. De Deyn, Johan A. den Boer, and Ulrich L. M. Eisel. 2012. “Lipocalin 2: Novel Component of Proinflammatory Signaling in Alzheimer’s Disease.” *The FASEB Journal* 26 (7): 2811.

Newcombe, Estella A., Judith Camats-Perna, Mallone L. Silva, Nicholas Valmas, Tee Jong Huat, and Rodrigo Medeiros. 2018. “Inflammation: The Link between Comorbidities, Genetics, and Alzheimer’s Disease.” *Journal of Neuroinflammation* 15 (1): 276.

Ojeda-Juárez, Daniel, Rohan Shah, Jerel Adam Fields, Indira S. Harahap-Carrillo, Jeffrey Koury, Ricky Maung, Benjamin B. Gelman, Bas J. Baaten, Amanda J. Roberts, and Marcus Kaul. 2020. “Lipocalin-2 Mediates HIV-1 Induced Neuronal Injury and Behavioral Deficits by Overriding CCR5-Dependent Protection.” *Brain, Behavior, and Immunity* 89 (October): 184–99.

Palenski, Tammy L., Christine M. Sorenson, Colin R. Jefcoate, and Nader Sheibani. 2013. “Lack of Cyp1b1 Promotes the Proliferative and Migratory Phenotype of Perivascular Supporting Cells.” *Laboratory Investigation; a Journal of Technical Methods and Pathology* 93 (6): 646–62.

Palop, Jorge J., and Lennart Mucke. 2010. “Amyloid-β–induced Neuronal Dysfunction in Alzheimer’s Disease: From Synapses toward Neural Networks.” *Nature Neuroscience* 13 (7): 812–18.

Park, Laibaik, Karin Hochrainer, Yorito Hattori, Sung Ji Ahn, Antoine Anfray, Gang Wang, Ken Uekawa, et al. 2020. “Tau Induces PSD95-Neuronal NOS Uncoupling and Neurovascular Dysfunction Independent of Neurodegeneration.” *Nature Neuroscience* 23 (9): 1079–89.

Pawelec, Graham, Arne Akbar, Calogero Caruso, Rafael Solana, Beatrix Grubeck-Loebenstein, and Anders Wikby. 2005. “Human Immunosenescence: Is It Infectious?” *Immunological Reviews* 205 (June): 257–68.

Perry, V. Hugh, Colm Cunningham, and Clive Holmes. 2007. “Systemic Infections and Inflammation Affect Chronic Neurodegeneration.” *Nature Reviews. Immunology* 7 (2): 161–67.

Pioli, Elsa Y., Brianna N. Gaskill, Gary Gilmour, Mark D. Tricklebank, Sophie L. Dix, David Bannerman, and Joseph P. Garner. 2014. “An Automated Maze Task for Assessing Hippocampus-Sensitive Memory in Mice.” *Behavioural Brain Research* 261 (100): 249.

Price, Brittani R., Christopher M. Norris, Pradoldej Sompol, and Donna M. Wilcock. 2018. “An Emerging Role of Astrocytes in Vascular Contributions to Cognitive Impairment and Dementia.” *Journal of Neurochemistry* 144 (5): 644–50.

Qiu, Wei Qiao, and Marshal F. Folstein. 2006. “Insulin, Insulin-Degrading Enzyme and Amyloid-Beta Peptide in Alzheimer’s Disease: Review and Hypothesis.” *Neurobiology of Aging* 27 (2): 190–98.

Quintanilla. 2004. “Interleukin-6 Induces Alzheimer-Type Phosphorylation of Tau Protein by Deregulating the cdk5/p35 Pathway.” *Experimental Cell Research* 295 (1): 245–57.

Readhead, Ben, Jean-Vianney Haure-Mirande, Cory C. Funk, Matthew A. Richards, Paul Shannon, Vahram Haroutunian, Mary Sano, et al. 2018. “Multiscale Analysis of Independent Alzheimer’s Cohorts Finds Disruption of Molecular, Genetic, and Clinical Networks by Human Herpesvirus.” *Neuron* 99 (1): 64–82.e7.

Rice, Rachel A., Nicole C. Berchtold, Carl W. Cotman, and Kim N. Green. 2014. “Age-Related Downregulation of the CaV3.1 T-Type Calcium Channel as a Mediator of Amyloid Beta Production.” *Neurobiology of Aging* 35 (5): 1002–11.

Saeed, Sadia, Jessica Quintin, Hindrik H. D. Kerstens, Nagesha A. Rao, Ali Aghajanirefah, Filomena Matarese, Shih-Chin Cheng, et al. 2014. “Epigenetic Programming of Monocyte-to-Macrophage Differentiation and Trained Innate Immunity.” *Science* 345 (6204): 1251086.

Salimi, Hamid, and Robyn S. Klein. 2019. “Disruption of the Blood-Brain Barrier During Neuroinflammatory and Neuroinfectious Diseases.” In *Neuroimmune Diseases: From Cells to the Living Brain*, edited by Hiroshi Mitoma and Mario Manto, 195–234. Cham: Springer International Publishing.

Sangwung, Panjamaporn, Guangjin Zhou, Lalitha Nayak, E. Ricky Chan, Sandeep Kumar, Dong-Won Kang, Rongli Zhang, et al. 2017. “KLF2 and KLF4 Control Endothelial Identity and Vascular Integrity.” *JCI Insight* 2 (4): e91700.

Santos, Cláudia Y., Peter J. Snyder, Wen-chih Wu, Mia Zhang, Ana Echeverria, and Jessica Alber. 2017. “Pathophysiologic Relationship between Alzheimer’s Disease, Cerebrovascular Disease, and Cardiovascular Risk: A Review and Synthesis.” *Alzheimer’s & Dementia: Diagnosis, Assessment & Disease Monitoring*. https://doi.org/10.1016/j.dadm.2017.01.005.

Sasaki-Hamada, Sachie, Masaatsu Ikeda, and Jun-Ichiro Oka. 2019. “Glucagon-like Peptide-2 Rescues Memory Impairments and Neuropathological Changes in a Mouse Model of Dementia Induced by the Intracerebroventricular Administration of Streptozotocin.” *Scientific Reports*. https://doi.org/10.1038/s41598-019-50167-3.

Serrano-Pozo, Alberto, Matthew L. Mielke, Teresa Gómez-Isla, Rebecca A. Betensky, John H. Growdon, Matthew P. Frosch, and Bradley T. Hyman. 2011. “Reactive Glia Not Only Associates with Plaques but Also Parallels Tangles in Alzheimer’s Disease.” *The American Journal of Pathology* 179 (3): 1373–84.

Siemsen, B. M., J. D. Landin, J. A. McFaddin, K. N. Hooker, L. J. Chandler, and M. D. Scofield. 2020. “Chronic Intermittent Ethanol and Lipopolysaccharide Exposure Differentially Alter Iba-1-Derived Microglia Morphology in the Prelimbic Cortex and Nucleus Accumbens Core.” *bioRxiv*. https://doi.org/10.1101/566034.

Silveira, Vivian T., Daniel Castro Medeiros, Jivago Ropke, Patricia A. Guidine, Gustavo H. Rezende, Marcio Flavio D. Moraes, Eduardo Mazoni A, Danielle Macedo, Fabricio A. Moreira, and Antonio Carlos P. Oliveira. 2017. “Effects of Early or Late Prenatal Immune Activation in Mice on Behavioral and Neuroanatomical Abnormalities Relevant to Schizophrenia in the Adulthood.” *International Journal of Developmental Neuroscience*. https://doi.org/10.1016/j.ijdevneu.2017.01.009.

Sochocka, Marta, Katarzyna Zwolińska, and Jerzy Leszek. 2017. “The Infectious Etiology of Alzheimer’s Disease.” *Current Neuropharmacology* 15 (7): 996–1009.

Song, Juhyun, and Oh Yoen Kim. 2018. “Perspectives in Lipocalin-2: Emerging Biomarker for Medical Diagnosis and Prognosis for Alzheimer’s Disease.” *Clinical Nutrition Research*. https://doi.org/10.7762/cnr.2018.7.1.1.

Soscia, Stephanie J., James E. Kirby, Kevin J. Washicosky, Stephanie M. Tucker, Martin Ingelsson, Bradley Hyman, Mark A. Burton, et al. 2010. “The Alzheimer’s Disease-Associated Amyloid Beta-Protein Is an Antimicrobial Peptide.” *PloS One* 5 (3): e9505.

Stranahan, Alexis M., and Mark P. Mattson. 2010. “Selective Vulnerability of Neurons in Layer II of the Entorhinal Cortex during Aging and Alzheimer’s Disease.” *Neural Plasticity* 2010 (December): 108190.

Streit, Wolfgang J., Sharon A. Walter, and Nathan A. Pennell. 1999. “Reactive Microgliosis.” *Progress in Neurobiology*. https://doi.org/10.1016/s0301-0082(98)00069-0.

Thal, Dietmar Rudolf, Estifanos Ghebremedhin, Udo Rüb, Haruyasu Yamaguchi, Kelly Del Tredici, and Heiko Braak. 2002. “Two Types of Sporadic Cerebral Amyloid Angiopathy.” *Journal of Neuropathology and Experimental Neurology* 61 (3): 282–93.

Ting, Jenny. 2001. “Faculty Opinions Recommendation of Recognition of Double-Stranded RNA and Activation of NF-kappaB by Toll-like Receptor 3.” *Faculty Opinions – Post-Publication Peer Review of the Biomedical Literature*. https://doi.org/10.3410/f.1001215.16876.

Toledo, Jon B., Steven E. Arnold, Kevin Raible, Johannes Brettschneider, Sharon X. Xie, Murray Grossman, Sarah E. Monsell, Walter A. Kukull, and John Q. Trojanowski. 2013. “Contribution of Cerebrovascular Disease in Autopsy Confirmed Neurodegenerative Disease Cases in the National Alzheimer’s Coordinating Centre.” *Brain*. https://doi.org/10.1093/brain/awt188.

Town, Terrence, David Jeng, Lena Alexopoulou, Jun Tan, and Richard A. Flavell. 2006. “Microglia Recognize Double-Stranded RNA via TLR3.” *Journal of Immunology* 176 (6): 3804–12.

Tzeng, Nian-Sheng, Chi-Hsiang Chung, Fu-Huang Lin, Chien-Ping Chiang, Chin-Bin Yeh, San-Yuan Huang, Ru-Band Lu, et al. 2018. “Anti-Herpetic Medications and Reduced Risk of Dementia in Patients with Herpes Simplex Virus Infections—a Nationwide, Population-Based Cohort Study in Taiwan.” *Neurotherapeutics: The Journal of the American Society for Experimental NeuroTherapeutics* 15 (2): 417–29.

Van Hove, Hannah, Liesbet Martens, Isabelle Scheyltjens, Karen De Vlaminck, Ana Rita Pombo Antunes, Sofie De Prijck, Niels Vandamme, et al. 2019. “A Single-Cell Atlas of Mouse Brain Macrophages Reveals Unique Transcriptional Identities Shaped by Ontogeny and Tissue Environment.” *Nature Neuroscience* 22 (6): 1021–35.

Walkera, Frederick Rohan, Michael Nilsson, and Kimberley Jones. 2013. “Acute and Chronic Stress-Induced Disturbances of Microglial Plasticity, Phenotype and Function.” *Current Drug Targets* 14 (October): 1262.

Walker, F. Rohan, Sarah B. Beynon, Kimberley A. Jones, Zidan Zhao, Ratchaniporn Kongsui, Murray Cairns, and Michael Nilsson. 2014. “Dynamic Structural Remodelling of Microglia in Health and Disease: A Review of the Models, the Signals and the Mechanisms.” *Brain, Behavior, and Immunity* 37 (March): 1–14.

Wang, Feixue, Yu Cao, Lina Ma, Hui Pei, Wolf Dieter Rausch, and Hao Li. 2018. “Dysfunction of Cerebrovascular Endothelial Cells: Prelude to Vascular Dementia.” *Frontiers in Aging Neuroscience* 10 (November): 376.

Williams, J., M. Dragunow, P. Lawlor, S. Mason, W. C. Abraham, J. Leah, R. Bravo, J. Demmer, and W. Tate. 1995. “Krox20 May Play a Key Role in the Stabilization of Long-Term Potentiation.” *Brain Research. Molecular Brain Research* 28 (1): 87–93.

Xie, Yan-Chun, Zhao-Hui Yao, Xiao-Li Yao, Jian-Zhen Pan, Shao-Feng Zhang, Yong Zhang, and Ji-Chang Hu. 2018. “Glucagon-Like Peptide-2 Receptor Is Involved in Spatial Cognitive Dysfunction in Rats After Chronic Cerebral Hypoperfusion.” *Journal of Alzheimer’s Disease: JAD* 66 (4): 1559–76.

Yanguas-Casás, Natalia. 2020. “Physiological Sex Differences in Microglia and Their Relevance in Neurological Disorders.” *Neuroimmunol. Neuroinflamm* 7: 13–22.

Yin, Jie, Katherine L. Valin, Michael L. Dixon, and Jianmei W. Leavenworth. 2017. “The Role of Microglia and Macrophages in CNS Homeostasis, Autoimmunity, and Cancer.” *Journal of Immunology Research* 2017 (December). https://doi.org/10.1155/2017/5150678.

Young, Kimberly, and Helena Morrison. 2018. “Quantifying Microglia Morphology from Photomicrographs of Immunohistochemistry Prepared Tissue Using ImageJ.” *Journal of Visualized Experiments: JoVE*, no. 136 (June). https://doi.org/10.3791/57648.

Tables

Table 1: Plasma inflammatory panel in aging PP and NN mice

Age	Group	Chemokine (pg/ml)	Inflammatory cytokines (pg/ml)		
		MCP-1	IL-6	TNF-From	IL-10
3 months	NN	11.1±0.7	7.1±0.2	3.8±0.3	2.7±0.2
	PP	19.8±1.9	8.3±0.3	3.3±0.2	7.7±0.7
	Fold change	1.8*	1.2	0.9	2.9*
6 months	NN	12.1±3.4	2.4±0.2	3.2±0.2	4.1±1.6
	PP	29.8±11.9	15.8±10.6	6.8±0.7	12.0±3.6
	Fold change	2.5*	6.5**	2.1**	2.9**
9 months	NN	35.7±26.9	243.4±187.5	8.9±0.7	16.4±4.7
	PP	17.2±8.4	1464.2±184.5	8.3±0.2	9.1±1.9
	Fold change	0.5	6.1**	0.9	0.6
16 months	NN	2.5±1.0	6.5±0.1	8.0±0.3	10.5±2.1
	PP	2.2±0.5	6.9±0.3	7.9±0.2	4.7±1.7
	Fold change	0.9	1.1	1.0	0.5

Data are represented as mean ± SEM. NN= prenatal& postnatal saline injected controls, PP = prenatal and postnatal PolyI:C treated mice. 3 months (NN=4, PP=4), 6 months (NN=8, PP=8), 9 & 16 months (NN, PP=5 each). *p <0.05, **p<0.01 versus control group, Student`s t-test

Table 2 Validation of transcripts via qPCR in aging PP mice as compared to age-matched NN

Age	Gene	Log2FC	FC	Regulation	Pathways& Functions	P value
3 nonths	*Lcn2**		-0.32	Down	Inflammatory signaling; dendritic spine pruning	0.02
	*Kcnj2**		1.01	-	Ionic conductance; slow inhibitory current	0.95
	*Egr2**	-0.1 (NS)	0.9	-	Early immediate gene	0.94
	*Plin4**	0.6 (NS)	3.1	-	Lipid metabolism	0.23
	Cacna1g	-0.6	0.9	-	Calcium channel	0.77
6 nonths	*Lcn2*		-0.6	-	Inflammatory signaling; dendritic spine pruning	0.70
	Glpr2	-3.7	-0.2	Down	Akt-mTOR; synaptic activity, neuroprotection	0.03
	Ide	0.5	1.6	-	Insulin signaling; Amyloid-b processing	0.16
	*Kcnj2**	0.1 (NS)	1.8	Up	Ionic conductance; slow inhibitory current	0.04
	*Plin4**	-0..23 (NS)	0.28	-	Lipid metabolism	0.49
9 nonths	*c-Jun*	-0.9	-1.8	Down	JNK3 pathway; IEG	0.05
	c-fos	-1.7	-3.2	Down	JNK3 pathway; IEG	0.002
	Notch1	-0.5	-2.5	Down	Notch signaling; synaptic plasticity	0.002
	*Kcnj2**	-0.7	-0.8	Down	Ionic conductance; slow inhibitory current	0.03
	*Egr2**	-0.9	-0.5	Down	IEG response; immune response	0.02
	*Lcn2**	2.0	2.6	Up	Inflammatory signaling; dendritic spine pruning	0.05
	*Plin4**	2.7	1.8	-	Lipid metabolism	0.24
	Klf4	-2.1	-0.43	Down	Inflammation, vascular intergrity	0.01
	Cyp1b1	1.6	2.4	Up	Cell adhesion, angiogenesis	0.07
	Angptl4	1.7	2.4	Up	Vascular permeability Lipid homeostasis	0.02
16 nonths	*Kcnj2**	-0.8	-0.8	-	Ionic conductance; slow inhibitory current	0.36
	*Egr2**	-1.2	-0.5	Down	IEG response; immune response	0.04
	*Lcn2**	5.6	4.5	Up	Inflammatory signaling; dendritic spine pruning	0.03
	*Plin4**	1.8	2.3	Up	Lipid metabolism	0.08
	Klf4	0.02	-0.08	-	Inflammation, vascular intergrity	0.82
	Cyp1b1	1.0	1.45	-	Cell adhesion, angiogenesis	0.28
	Angptl4	1.0	1.1	-	Vascular permeability Lipid homeostasis	0.47

FC=Fold Change; NS=non-significant DEG; * Shared genes with progressive changes in the PP versu NN

Table 3. Summary of Patients' cohort I

Stage	N. patients	F: M	Age (mean±SD)	Braak (mean ±SD)
CTL	9	5: 4	81± 8.8	1.0± 0.5
MOD	5	3: 2	85± 2.2	4.0± 1.6
AD	10	4: 6	82± 9.9	5.6± 0.5

CTL=healthy controls; MOD=moderate AD; AD=severe AD

Table 4. Summary of Patients' cohort II

Stage	N. patients	F: M	Age (mean±SD)	Braak (mean ±SD)
CTL	5	2: 3	80± 5.9	2.3± 0.5
VaD	6	3: 3	82± 3.5	4.0± 1.6

CTL=healthy controls; VaD=Vascular dementia

Figures

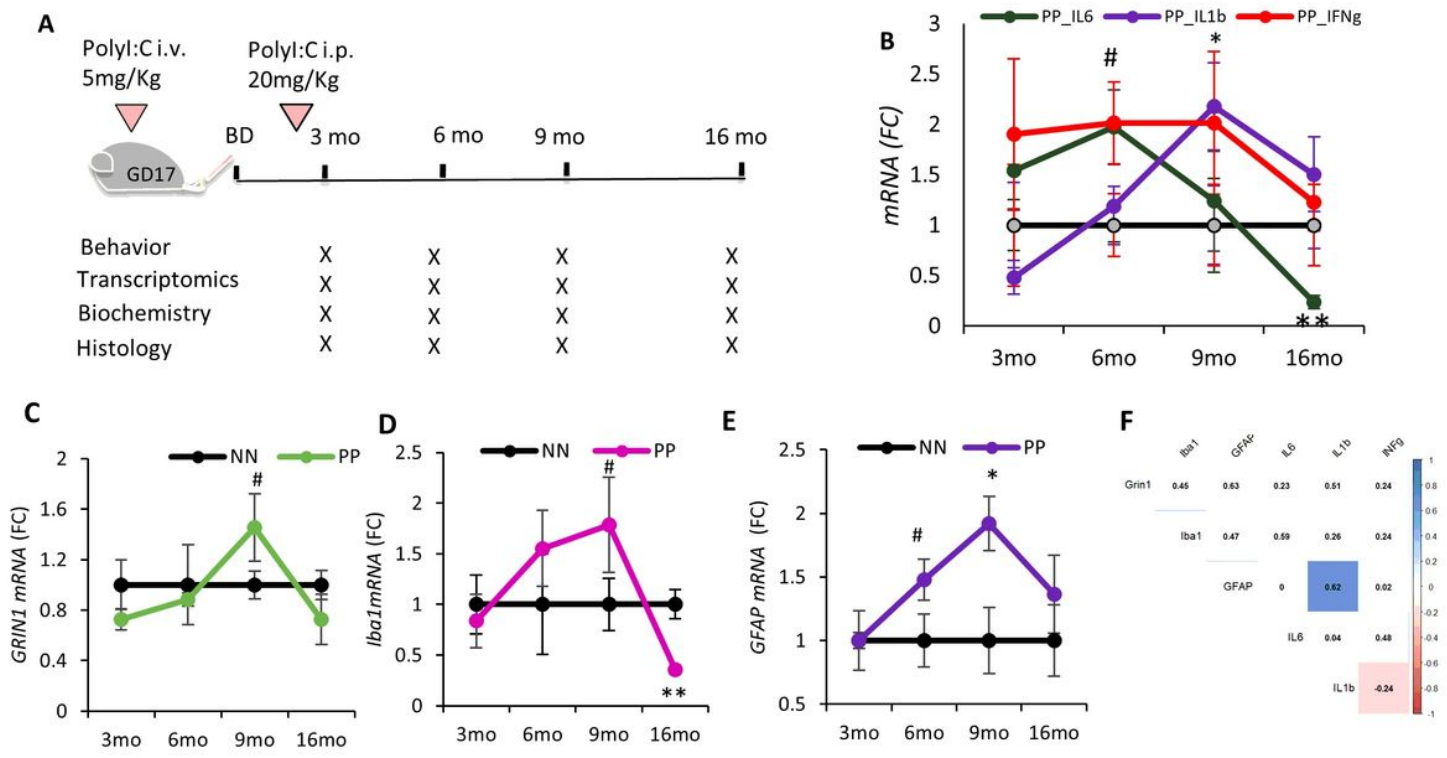

Figure 1

The neuroinflammatory evolution in aging PolyI:C mice. (A) Timeline of the experimental procedure and PolyI:C injections. (B) RT-PCR analysis of proinflammatory cytokines in the hippocampus after the PolyI:C treatment. Transcript analysis for (C) neuronal (GRIN1), (D) microglia (Iba1), and (E) astroglial (GFAP) markers. (F) The correlation matrix indicates the associations between time series of Grin1, Iba1, GFAP with the examined cytokines. Values represented as mean ± SEM, n=4-5 mice per age, and treatment. GD=gestational day, BD=birthday. *p<0.05, **p<0.005, #p=0.07. . Statistical significance based on two-way ANOVA/Bonferroni post hoc analysis.

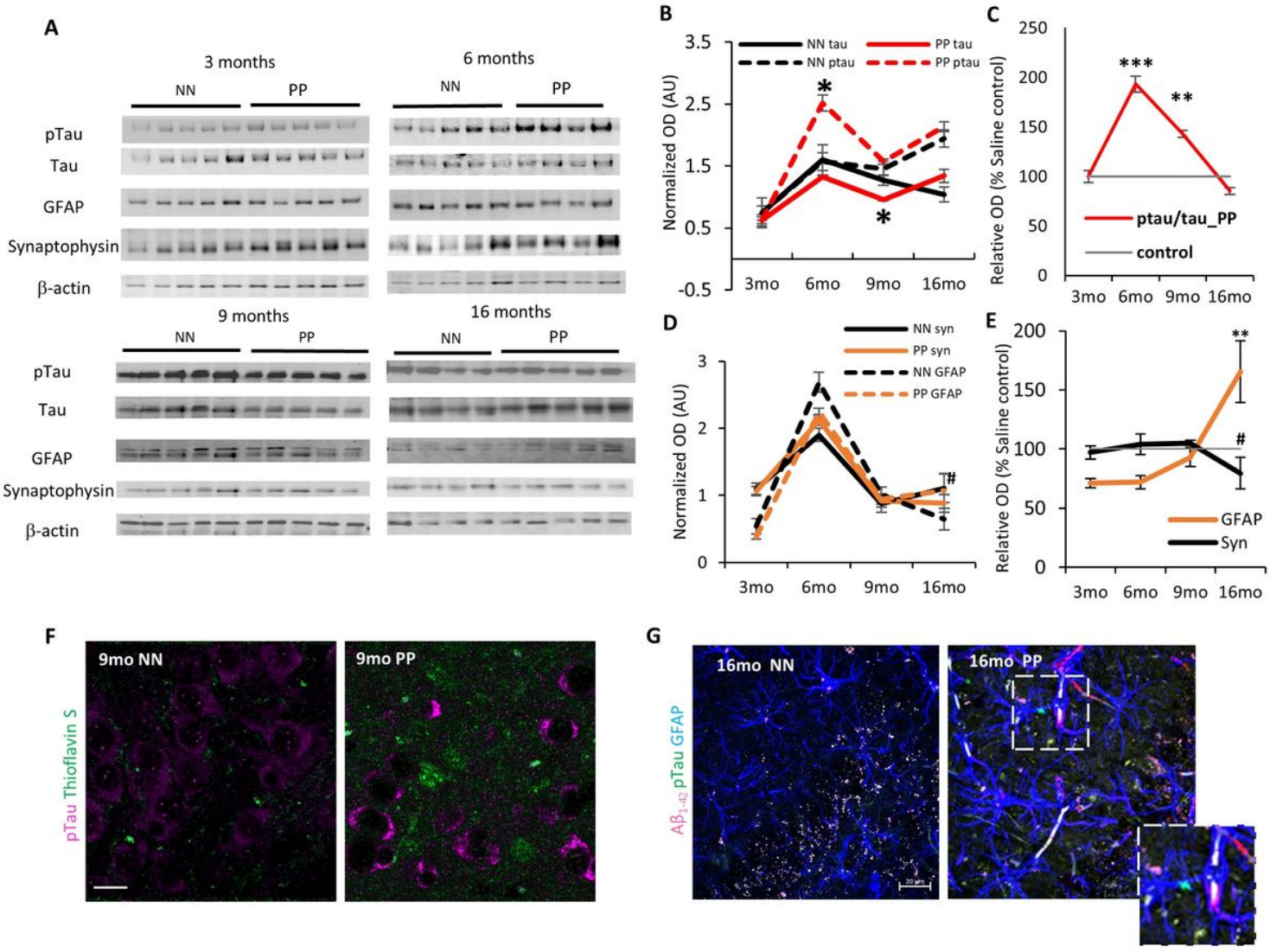

Figure 2

The Effect of PolyI:C on p-tau accumulation in the hippocampus. (A) Immunoblots of hippocampal lysate from PP and NN mice at 3, 6, 9, and 16 months, for p-tau, tau, GFAP, Synaptophysin. β-Actin was used as housekeeping control. (B, D) Relative quantification of ptau, tau, GFAP, and Synaptophysin represented in normalized optical density. (C, E) Percentage of relative changes of these proteins compared to the saline treated controls (NN). Representative immunostaining for (F) p-tau, Thioflavin S (9 months), and (G) Aβ1-42, p-tau, and GFAP at 16 months age group. Insert shows a GFAP positive processes with internalized Aβ1-42, p-tau aggregates. Scale bar in F is 45 μm, G is 20μm. Values represented as mean ± SEM, n=4-5 mice per age, and treatment. *p<0.05, **p<0.005, ***p<0.0005, #p=0.07.Statistical significance based on two-way ANOVA/Bonferroni post hoc analysis..

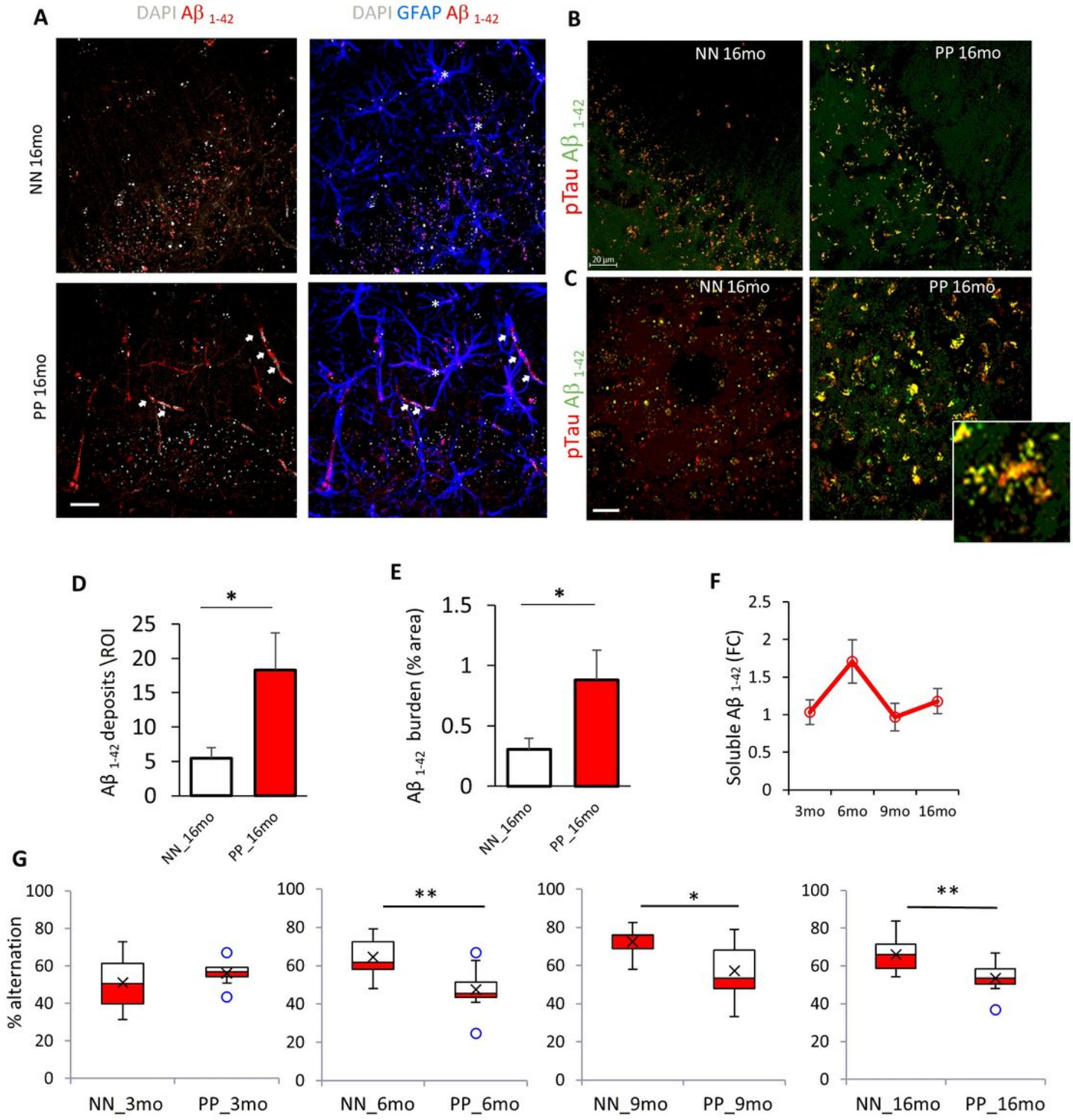

Figure 3

Amyloid fibrils in the hippocampus and entorhinal cortex with spatial memory deficits. (A) Double immunolabeling for A1-42 and GFAP shows internalization of amyloid in GFAP+ glia cells (stars) in NN and PP mice at 16 months and strong depositions of amyloid in vessels (white arrows) in PP mice. (B) Representative immunostaining of A1-42 and pTau231 in the hippocampus and (C) Entorhinal cortex of aged 16 months PP & NN controls. Insert showing p-Tau & A1-42 colocalization. (D) Quantification of

amyloid aggregates >5µm2 and (E) percentage area covered per region of interest (n=5-6 mice per condition & 4-5 ROI per mice). (F) Immunobead assay showing dynamic trend in soluble Aβ42 level fold changes in the cortical lysates relative to control (n=4-6 mice per age group & condition). (G) Box plots indicate a significant impairment in the percent of spontaneous alternation entry in PP mice compared from 6 to 16 months as compared to NN (n=7-10 mice per treatment and age). Values in bar charts and line graphs are represented as mean ± SEM. *p<0.05, **p<0.005 Student's t-test. Scale bar in A and B=20µm.

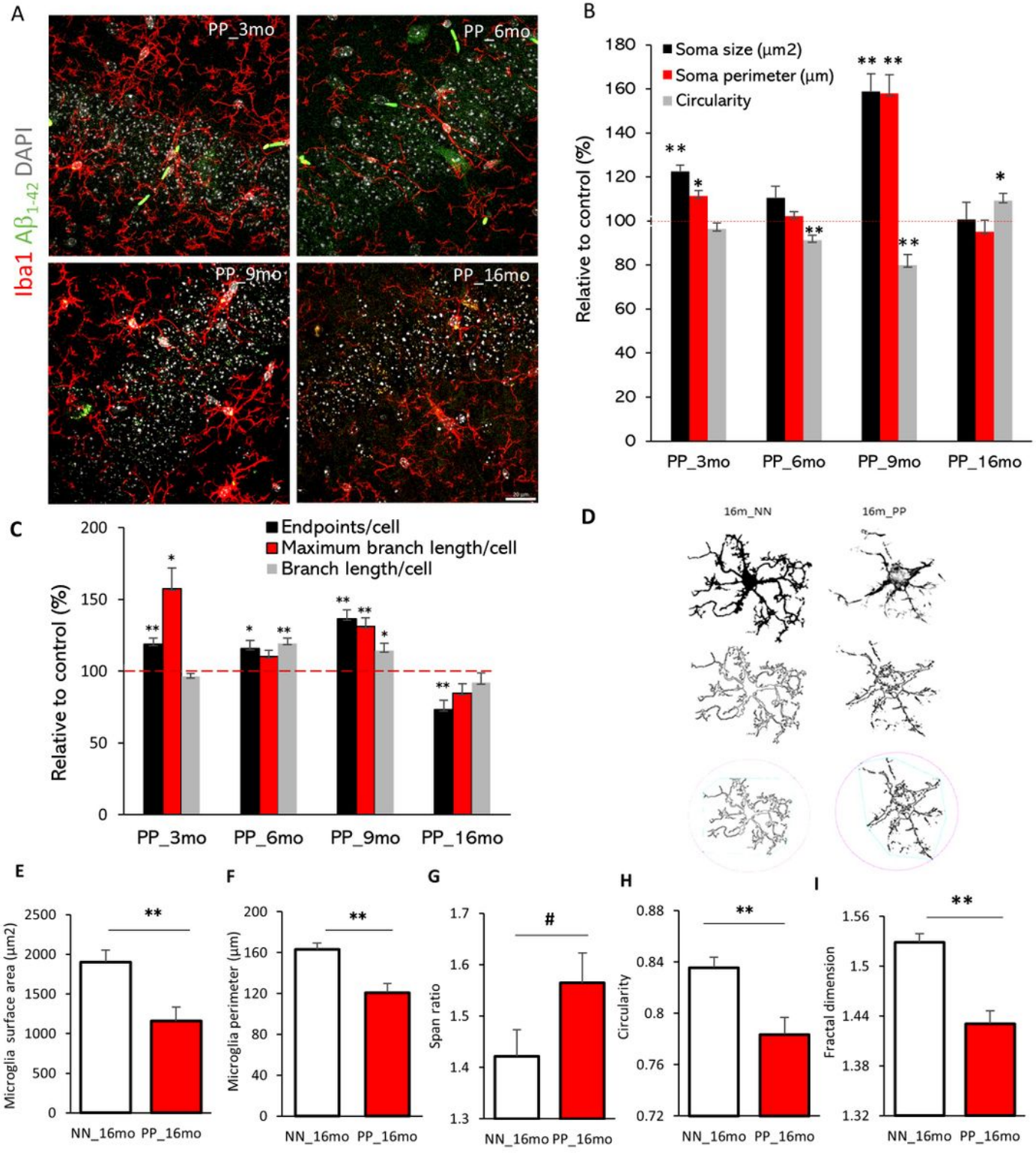

Figure 4

Longitudinal changes in hippocampal microglia. (A) Immunofluorescence staining for Iba1 and Aβ staining in the PolyI:C treated mice. (B) Dynamic changes in microglia soma size, perimeter and circularity were quantified in PolyI:C (PP) mice in different age groups. Data represented as % relative to controls. (n= 150-180 cells from 3-4 mice per group & condition in 3m, 6m stages; n=85 cells in 9m and n=55 cells at 16 months from 3 mice). (C) Bar chart of % relative values relative to controls for the average endpoints, maximum branch length, and branch length per cell. Red dotted line indicates the 100 percent control line (n=55-65 ROIs/3, 6, 9 months group and 25 ROIs/16 months; n=3 mice per age group and condition). (D) Example of fractal analysis of microglia from the hippocampus of PolyI:C and saline treated 16 months aged mice. Single-cell fractal analysis indicates the surface area (E) and perimeter (F) is decreased in PP mice, in contrast, the span ratio (G) showed a higher trend. PP mice showed a significant decrease in circularity (H) and fractal dimension (I) (n=45 cells from 3 mice per group and condition). Values in the bar charts are represented as mean ± SEM. #p=0.07,*p<0.05, **p<0.005 Student's t-test. Scale bar, A= 20μm.

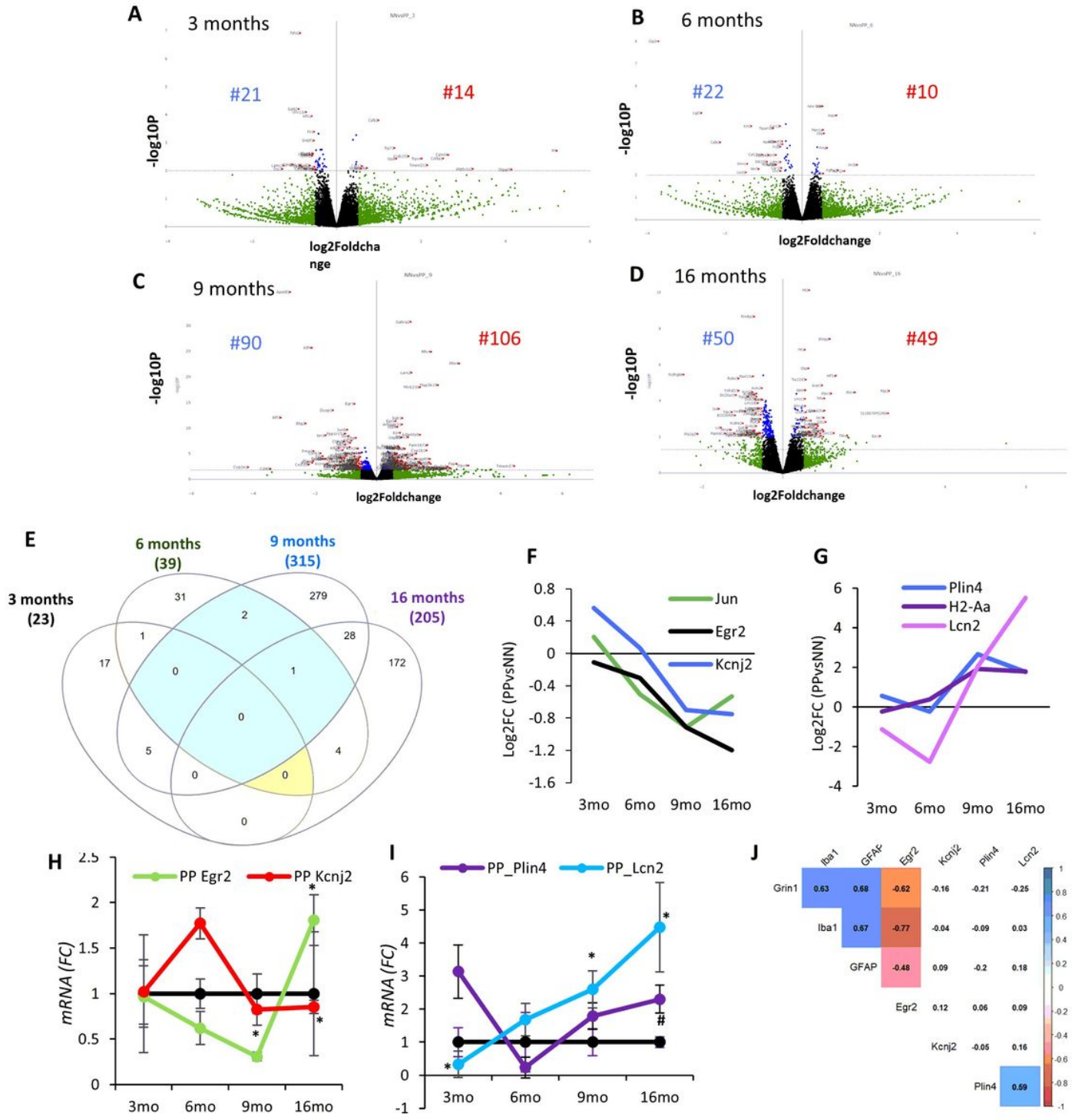

Figure 5

Bulk transcriptomics analysis of the hippocampus in the aging PolyI:C. Gene expression changes after the prenatal and early postnatal immune challenge. Volcano plot with log2-fold change (X-axis) and -log10 p-value (Y-axis) at different age groups (A) 3 months (B) 6months (C) 9 months and (D) 16 months in PP versus NN controls. Genes with log2 fold changes >0.5 are shown in green. Significantly regulated genes are shown in red (log2 fold change >0.5, p<0.05, left downregulated, and right upregulated). Genes with insignificant log2 fold changes <0.5 are shown in black [controls (NN) n=3/age, PolyI:C (PP)

n=3/age]. (E) Venn diagram indicating the number of uniquely and commonly affected genes in the aging hippocampus following prenatal and early postnatal PolyI:C (PP) treatment. Few common genes along with their Log2 Fold changes either (F) downregulated or (G) upregulated were plotted across staging. Transcript validation analysis for (H) Egr2 and Kcnj2 and (I) Plin4 and Lcn2. (J) Correlation matrix with highlighted significant association from 9 to 16 months among the differentially expressed cell-type markers (GFAP, Iba1, and Grin1) and Egr2, Kcnj2, Plin4 and Lcn2 between PolyI:C and saline controls [controls (NN), n=5/age, PolyI:C (PP) n=4-5/age]. Line plots show values as mean ± SEM. *=p<0.05, **=p<0.01, #=p@0.1, Student's t-test.

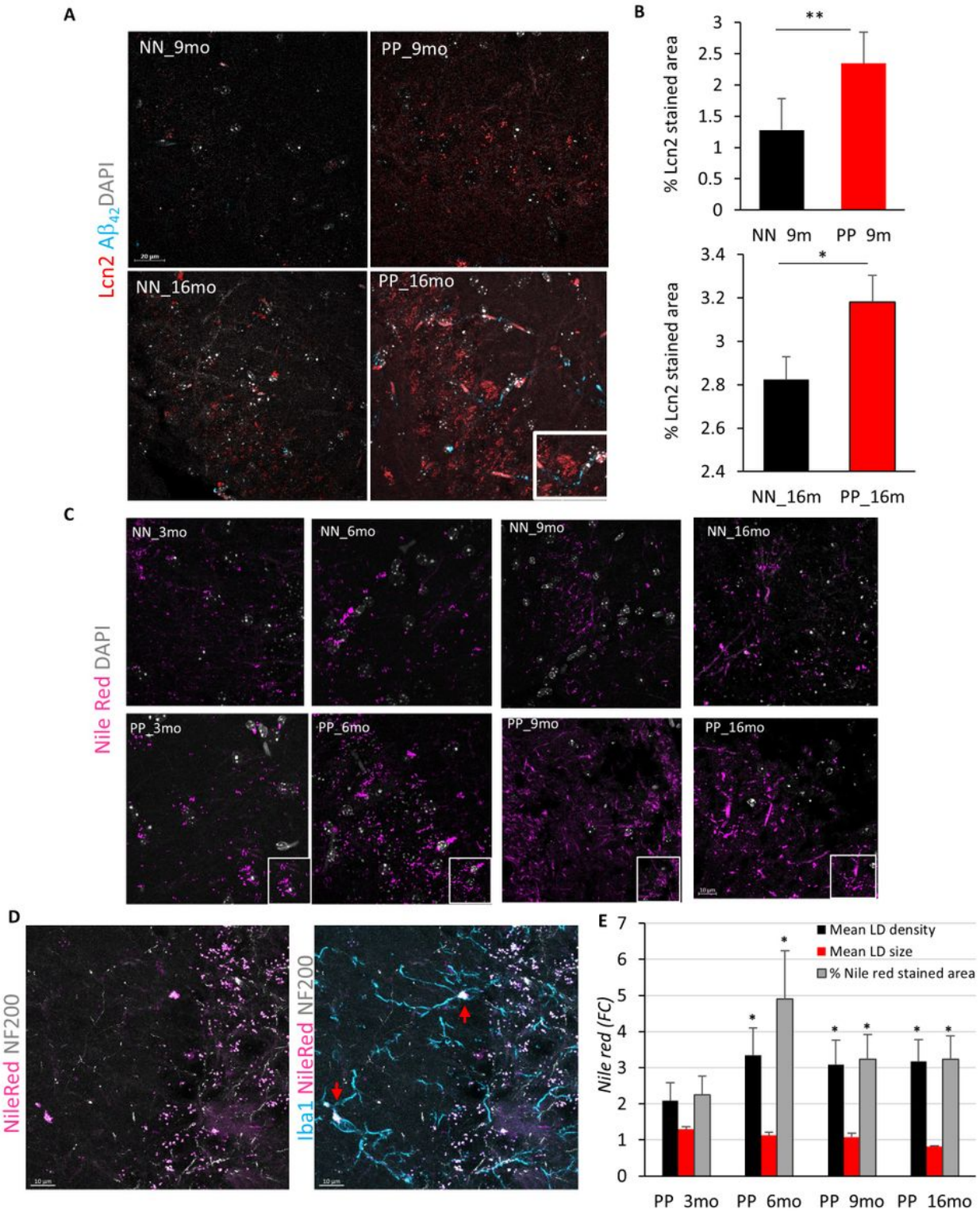

Figure 6

Effect of PolyI:C on the hippocampal Lcn2 & lipid droplet density. (A) Representative Lcn2, Aβ1-42 stained confocal images of saline and PolyI:C treated mice in 9 months and 16 months aged PP mice. Larger aggregates of Lcn2 (insert) visible at the 16 months PolyI:C exposed mice. (B) Quantification of % stained area indicates increased Lcn2 expression in the hippocampal CA3 field (n=4-6 mice for 9- and 16-months groups/treatment). (C) Nile red positive lipid droplet staining (violet) across aging in NN & PP mice. (D)

Representative triple fluorescence labeling with Nile Red, Iba1 (teal) and NF200 (grey) shows an overlap between the different marker localized lipid droplets in Iba1 positive cells. Arrows indicating NileRed+/Iba1+ cells. (E) Bar chart representing fold change values in the lipid droplet density, mean size, and % stained area per ROI measured. Data are represented as mean±SEM relative to control (n=3-4 mice per group/treatment). *p<0.05, **p<0.005, Student's t-test. Scale bar A= 20µm, C,E= 10µm.

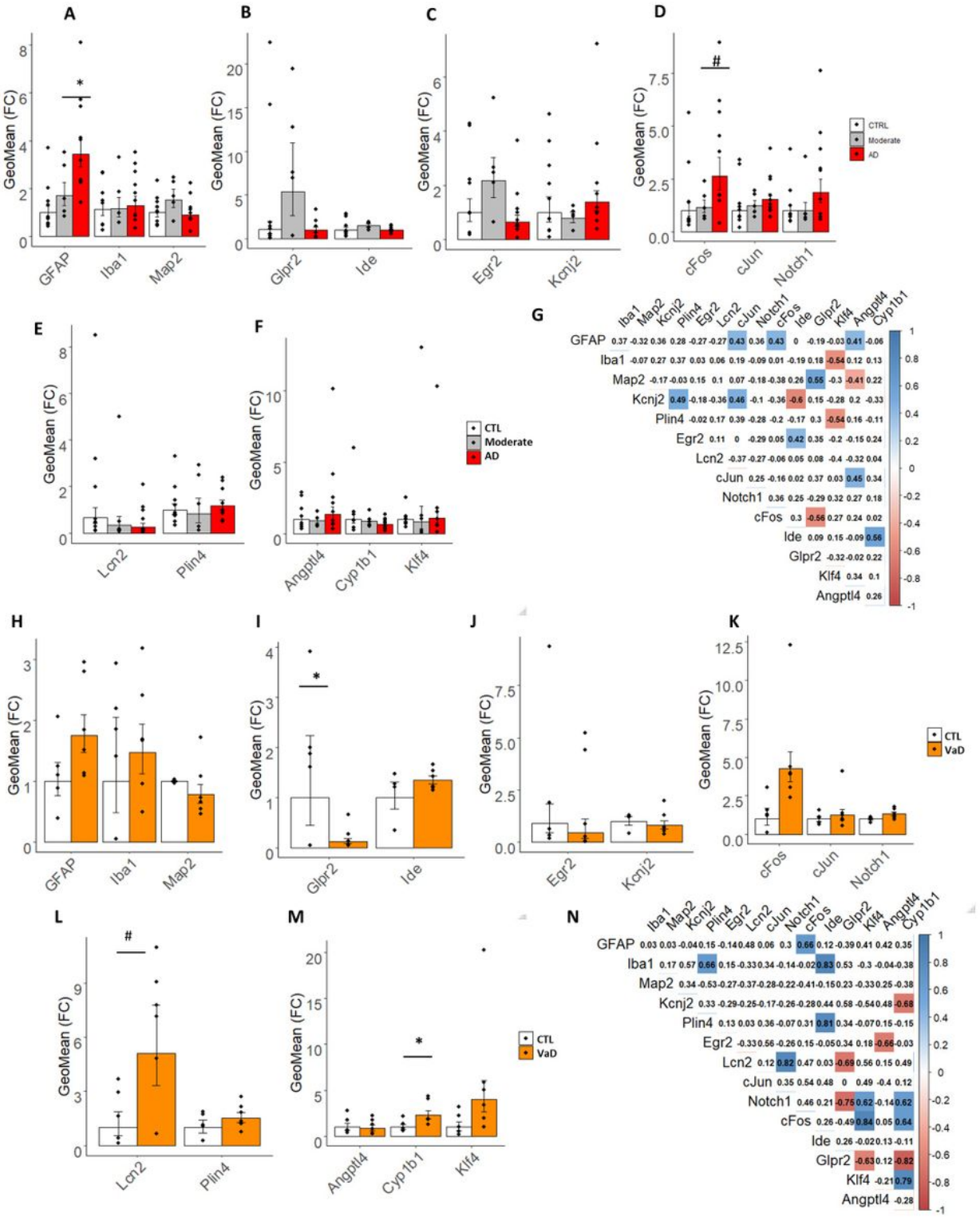

Figure 7

Target transcripts validation in the human brain specimen of patients with AD and VaD. Bar plots with Jitter showing the fold changes (FC) of the DEGs (A-F) in moderate AD and severe AD entorhinal cortices as compared to healthy controls (CTRL) and (H-N) in hippocampal sections from VaD as compared to healthy controls (CTRL). (A and H) FC of cell-type specific markers for astroglia (GFAP), microglia (Iba1) and neurons (MAP2). (B and I) FC of glucose metabolism markers, Glpr2 and Ide. (C and J) FC of plasticity markers, Egr2 and Kcnj2. (D and K) FC of cell signaling markers, c-fos, c-Jun and Notch1. (E and L) FC of inflammatory and metabolic markers, Lcn2 and Plin4. (F and M). FC of vascular markers, Angptl4, Cyp1b1 and Klf4. (G and N) Correlation matrix of the selected biomarkers in the two study cohorts. Data are represented as Geometric mean of fold change± Geometric SEM relative to healthy controls. *p<0.05, #p=0.054 based on one-way ANOVA/Bonferroni post hoc test correction. AD= Alzheimer's disease and VaD=vascular dementia.

Supplementary Files

This is a list of supplementary files associated with this preprint. Click to download.

- SupplFig1JNfl.tif
- SupplFig2JNfl.tif
- SupplFig3JNfl.tif
- SupplFig4JNfl.tif
- SupplFig5JNfl.tif
- SupplFigLegendsJNfl2020.docx
- SupplMaterialMethodJNfl2020.docx
- SupplTablesJNfl2020.docx